UNIVERSITÀ DEGLI STUDI DI PADOVA

FACOLTÀ DI SCIENZE MM. FF. NN.

Dipartimento di Geoscienze

Direttore Prof.ssa Cristina Stefani

TESI DI LAUREA MAGISTRALE IN GEOLOGIA E GEOLOGIA TECNICA

ARCHITECTURE AND SEISMIC MARKERS OF AN EXHUMED FAULT ZONE IN DOLOSTONES (FOIANA LINE, ITALIAN SOUTHERN ALPS)

Relatore: *Prof. Giulio Di Toro*

Correlatore: *Dott. Michele Fondriest*

Laureando: Stefano Aretusini

ANNO ACCADEMICO 2012/2013

Contents

Riassunto

Nelle sequenze sismiche di Bovec nel 1998 (faglia strike-slip, M_D 5.6), de L'Aquila nel 2009 (faglia normale, M_w 6.1) e dell'Emilia del 2012 (thrust, M_w 6.0) la rottura sismica del mainshock si è propagata, e diversi foreshock e aftershock sono nucleati, all'interno di sequenze sedimentarie costituite prevalentemente da rocce carbonatiche. Queste sequenze possono durare per molto tempo, da mesi ad anni, seguendo una evoluzione complessa in termini spaziotemporali, risultante probabilmente dalla geometria della faglia e del network di fratture, distribuzione delle rocce di faglia, iniezione di fluidi, ecc. Le tecniche sismologiche hanno risultati con scarsa risoluzione spaziale (gran parte dei casi circa 1 km), e non permettono la ricostruzione della complessità geometrica delle zone di faglia e della distribuzione delle rocce che le compongono. Da qui deriva la necessità di studi dedicati all'architettura delle faglie, a scale variabili dal chilometro al metro, sviluppate nei carbonati. Le informazioni così ottenute possono essere associate a dati sperimentali sulla meccanica della rottura e della frizione, per poi entrare in modelli di nucleazione e propagazione delle rotture sismiche, per lo studio del rischio sismico.

In questa tesi, ho usato un approccio multidisciplinare, che comprende telerilevamento, analisi strutturale di dettaglio sul terreno e studi microstrutturali per quantificare l'architettura della Linea della Foiana (qui definita Foiana Fault Zone, FFZ, in Val di Non, Alpi Meridionali, Italia). L'attività della FFZ inizia nel Permiano (soprattutto come faglia normale) e continua nel Miocene (come faglia traspressiva). Nella Val di Non, la FFZ intercetta le dolomie Triassiche della Fm. Di Sciliar, viene esumata da circa 1.5 a 2.5 km di profondità, andando verso nord. Nella parte meridionale, devia dalla direzione N-S piegando verso SW, evolvendo verso una anticlinale (tipo fault-propagation). Come sarà discusso in questo lavoro, la FFZ è stata interessata da attività sismica durante il Miocene, come supportato da prove

di terreno e microstrutturali. Nella parte di telerilevamento, grazie a modelli digitali di terreno ad alta risoluzione (da 1 a 2.5 metri), su base LIDAR, sono stati tracciati i lineamenti della FFZ e nelle zone adiacenti. Questi sono stati poi classificati sulla base della loro direzione media e quindi la loro distribuzione interpretata col modello di Riedel, fatto che ha confermato la FFZ come faglia sinistra. Il rilevamento strutturale di dettaglio è stato intrapreso in tre località (da sud: Carnalez, Salobbi e Doss de la Ceora), distribuite lungo un segmento della FFZ di 7 km, nella parte più meridionale della stessa. Sono state studiate sezioni parallele e perpendicolari alla direzione della faglia per misurare le giaciture e la spaziatura delle principali strutture e la distribuzione delle rocce di faglia. Un aspetto interessante è stata la presenza di grossi volumi (spessi fino a 300 m) di dolomie frantumate, con shear strain poco o per nulla presente, tagliate da superfici di slip a specchio (mirror-like). La presenza di clasti troncati dalle superfici a specchio, di clasti interessati da fratture radiali ("clasti esplosi"), suggerisce l'origine cosismica di queste rocce di faglia, coerentemente con i prodotti di esperimenti in condizioni di slip cosismico.

In generale, la giacitura ed il senso di shear delle faglie minori della FFZ evolvono da disperse, con componente inversa dominante nelle zone a sud (Carnalez) fino a disporsi subparallele con componente strike-slip predominante, a nord (Doss de la Ceora). Questo cambiamento significativo nell'architettura della FFZ va parallelamente alla riduzione in spessore delle rocce frantumate, da 300 metri presso Carnalez a meno di 200 metri, presso Doss de la Ceora. Queste variazioni nell'architettura lungo lo strike della FFZ sono interpretate come risultato del fault bend a sud o in termini di processi relativi alle rotture sismiche. Nel secondo caso, l'ampia dispersione delle giaciture e nel senso di shear, diversamente dalla parte più settentrionale, può riflettere gli effetti della direttività della rottura e della diversa profondità dell'attività sismica (aumento della dispersione con minore pressione di confinamento), come è stato osservato in recenti simulazioni sugli effetti del danneggiamento delle rotture sismiche. Infine si è osservato come le superfici di strato preesistenti siano un fattore principale nel controllo della nucleazione di superfici di slip, e del successivo ispessimento della zona di faglia durante l'avanzamento della deformazione.

Abstract

The earthquake sequences of Bovec 1998 (strike-slip focal mechanism, M_D 5.6), L'Aquila 2009 (normal, M_w 6.1) and Emilia 2012 (thrust, M_w 6.0) had the main shocks ruptures propagating and several foreshocks and aftershock nucleating within sedimentary successions mostly made of carbonatic rocks. These earthquake sequences are often long lasting (several months to years) and follow a complex spatio-temporal evolution, which is probably the result of the geometry of the fault-fracture network, fault rock distribution, ingression of fluids, etc. Seismic waves inversion analysis has limited spatial resolution (in most cases > 1 km), and does not allow to reconstruct the geometrical complexity of fault zones and the distribution of fault rocks. Here the need of dedicated studies, from metric to kilometric scale ("multi-scalar") of the architecture of faults hosted in carbonatic sedimentary rocks. This information, associated with mechanical data obtained from friction and rupture experiments, could be used in physically-based earthquake forecasting models and in simulation of seismic ruptures for earthquake hazard studies.

In this thesis, I used a multidisciplinary approach which includes remote sensing analysis, detailed geological field survey and microstructural studies to quantify the architecture of the 30 km long north-south striking Foiana Fault Zone (FFZ, Linea della Foiana *auctores*: Val di Non, Italian Southern Alps). The FFZ activity lasted from the Permian (mainly normal faulting) to the Miocene (mainly strike-slip faulting). In the Val di Non area, the FFZ is mainly hosted in Triassic dolostones (Sciliar Fm.), was exhumed from 1.5 km (southern segment) to 2.5 km (central segment) depth and, in his southern part, curves to the south-west into a restraining bend producing a fault-propagation anticline. As discussed here, the FFZ underwent seismic activity during the Miocene as attested by field and microstructural evidences. The remote sensing analysis, thanks to the high resolution (2.5 to 1 m)

of the LIDAR-based digital terrain models images, allowed a detailed reconstruction of the structural lineaments of the FFZ and neighbor areas. The lineaments were organized in groups based on their strike. The Riedel-shear model was used to interpret their geometrical arrangement, which was consistent with the left-lateral kinematics of the FFZ. Detailed structural field geology survey (which included systematic rock sampling) was performed in three localities (from south to the north: Carnalez, Salobbi and Doss de la Ceora) covering a ca. 7 km long segment of the southern part of the FFZ. I traced sections parallel and orthogonal to fault strike to determine the attitude and spacing of the main structural features (faults, joints, bedding, etc.) and the distribution and characteristics of the fault zone rocks. An intriguing aspect was the presence of large volumes (up to 300 m in thickness) of in-situ shattered (fracture density from 3 cm to few mm) dolostones with negligible or null shear strain, cut by ultracataclastic slipping zones with mirror-like surfaces. The presence of clasts truncated by the mirror-surfaces and of clasts with radial fractures ("exploded" grains) immersed in the fine matrix of the ultracataclasites, is indicative of the seismic origin of these fault rocks, consistently with recent experiments reproducing seismic slip deformation conditions.

In general, the attitude of the minor faults of the FFZ evolves from scattered with dominant reverse dip-slip reverse component in the southern exposures (Carnalez) to sub-parallel faults with dominant strike-slip towards the northern exposures (Doss de la Ceora). This major change in the architecture of the FFZ is concomitant with a decrease in the thickness of the damage zone (in-situ shattered dolostones) from 300 m in Carnalez to 200 m in Doss de la Ceora. These architectural along strike variations are here interpreted as the result of the presence of southern fault bend or of dynamic coseismic rupture processes. In the latter case, the larger scatter in the attitude (and sense of shear) of the fault-fracture network with respect to the northern exposures may reflect rupture directivity effects and the different depth of seismic faulting (larger the pressure confinement, larger the scatter of the attitude of the faults), consistently with recently published earthquake simulations models. Lastly, the pre-existing bedding surfaces appeared to be primary factor in controlling the nucleation of slip surfaces and fault zone thickening and growth during progressive deformation.

Chapter 1

Introduction

The investigation of the architecture of fault zones is one of the main research topics in structural geology, given its relevance in the exploitation of hydrocarbon, geothermal and water resources, in the disposal and storage of materials (CO_2, methane, nuclear waste, wastewater, etc.), in the engineering (tunnels, etc.) and mining (hydrothermal mineralizations, etc.) practice and in seismic hazard. The architecture of a fault zone comprehends the geometry of the fault-fracture network, the geometry of individual fault surfaces and the distribution of fault rocks. According to Caine [Caine et al., 1996], the architecture of an ideal fault zone consists of three main elements:

- the fault core: this is the rock volume where most of displacement of the fault is accommodated, and it contains one or more individual slip zones, often bounded by slip surfaces with variable roughness;

- the damage zone: the volume of fractured rock surrounding the fault core, cut by few discontinuous secondary faults. The displacement accommodated by the damage zone is negligible;

- the host rock: the protolith, dominated by primary structures depending on rock-type.

The spatial distribution of the fault rocks controls the hydraulic behavior and the physical properties (resistivity, acoustic impedence, etc.) of a fault zone. Depending on the relative volume (length, lateral continuity, thicknesses) and permeability
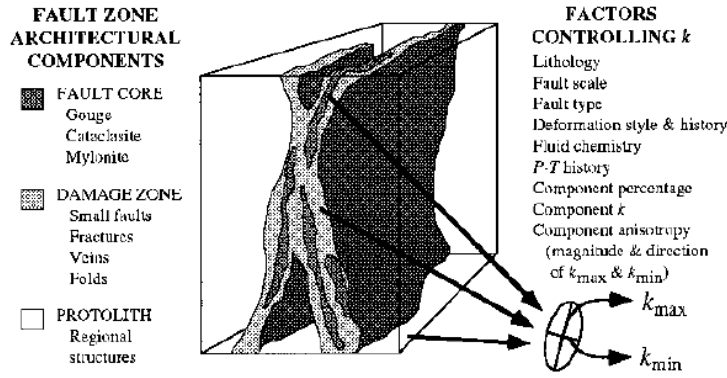
Figure 1. Conceptual model of fault zone with protolith removed (after Chester and Logan, 1986; Smith et al., 1990). Ellipse represents relative magnitude and orientation of the bulk two-dimensional permeability (k) tensor that might be associated with each distinct architectural component of fault zone.

Fig. 1.1: Architecture of an ideal fault [Caine et al., 1996].

properties of the fault core with respect to the damage zone, some conceptual models are presented for fault-related fluid infiltration and flow. For instance, permeability k controls fluid migration in reservoirs and geothermal fields where the fault core and the damage zone are distinct structural and hydrogeologic units: weather a fault acts as a conduit, a barrier or a barrier-conduit is controlled by the relative percentage of the fault core and damage zone structures and variability in grain size and fracture permeability (Fig.1.1).

Relevant for the topics addressed in this thesis, the fault zone architecture plays a key role in earthquake mechanics. The nucleation, propagation and arrest of a seismic rupture is controlled by the geometry of the fault zone (complexity of the fault-fracture network) and the distribution and type of fault rock materials [Scholz, 2002, Wibberley et al., 2008]. Indeed, fault surfaces are rough and the architecture of fault zones is greatly variable and heterogeneous because of the distribution of rocks (velocity-weakening vs. velocity-strengthening materials), the presence of pre-existing geometrical features (bedding, joints, etc.) and the degree of "maturity" of the fault (affected by fluid-rock interaction, displacement, etc.) [Wibberley et al., 2008, Faulkner et al., 2010]. All the above geometrical and mechanical heterogeneities, together with the style of deformation (compressive vs. extensional) result in difference in styles of seismicity: for instance, foreshocks sequences seem more common in extensional than in compressive regimes [Abercrombie and Mori, 1996]. Large-scale fault architecture studies show how the relay zones, fault bends,

and all the structures linking the different fault segments, are obstacles of the rupture propagation and so control the energy budget of the entire earthquake, determining the maximum size of the rupture [King and Nábělek, 1985, Wesnousky, 2006]. The lateral continuity also affects the speed of a seismic rupture: maximum speeds are achieved by supershear ruptures, which require straight and continuous fault segments [Bouchon et al., 2010]. Such supershear ruptures have been proposed as responsible of the shockwaves producing pulverized fault rocks [Doan and Gary, 2009].

In particular, the seismicity in the Mediterranean area (Italy, Greece, Turkey, Israel, Algeria, etc.) is often hosted in thick carbonate sequences, as was the case of the Friuli 1976 (mainshock M_w 6.4) or of the more recent L'Aquila 2009 (M_w 6.1) and Emilia 2012 (M_w 6.0) earthquake sequences [Chiaraluce et al., 2011, Valoroso et al., 2013]. Even if the lithology at the hypocentral depths of the main shocks of these three sequences remains debated, surely the rupture of the main shock propagated and many of the foreshocks and of the aftershocks nucleated in carbonate-built sedimentary rocks. In the Friuli 1976, L'Aquila 2009 and Emilia 2012 earthquake sequences, several sedimentary rock formations were made by dolostones. Here the need to investigate exhumed fault zone hosted in carbonate-built rocks and in particular in dolostones. This resulted, in the last years, in several studies of fault zones hosted in carbonates which highlighted the geometrical complexity of this fault zones and the role of geometric precursors (bedding, stylolitic surfaces, etc.) in controlling the architecture of the fault zone [Billi et al., 2003, Agosta and Aydin, 2006]. Importantly, to date there is not yet a satisfactory physical motivation for the differences related to individual earthquakes and to earthquake sequences. One reason for this is the lack (or paucity) of quantitative measurements of fundamental geometrical properties of fault zones and fault networks, which prevents these elements being included in numerical models.

But a further main limitation in the study of exhumed faults is to ascertain the origin of the studied fault rocks [Cowan, 1999]. Faults can be seismic but also aseismic (i.e., they accommodated slip without generating seismic waves recorded by broad-band seismometers) in origin. And the same fault zone records different stages of the seismic cycle, coseismic (rupture propagation at kms^{-1} and slip rate

at ms^{-1}) and aseismic (pre-seismic and post-seismic slip at slip rates of probably well below than 1 ms^{-1}). Clearly, the large number of earthquake sequences hosted in carbonate-built sedimentary rocks suggests that microstructures associated to seismic ruptures should be a quite common feature. Here the need to recognize microstructural features in carbonate-built fault zone rocks that record ancient seismic ruptures. This has been the main goal of several recent field and experimental studies dedicated to calcite- [Han et al., 2007,Smith et al., 2011,Smith et al., 2013,Viganò et al., 2011,Siman-Tov et al., 2013] and dolomite-in-composition [De Paola et al., 2011,Fondriest et al., 2013] brittle fault rocks. Moreover, microstructural, mineralogical and geochemical studies of experimental and natural slip zones can unravel the processes operating during the seismic slip [Niemeijer et al., 2012]. In the case of dolomite, very recent experimentally-based studies suggest that mirror-like surfaces hosted in highly fragmented rocks could be the result of slip at seismic rates [Fondriest et al., 2013]. The interest in these studies is also that they allow to determine the fault strength at seismic slip rates, which controls the dynamics of earthquake ruptures but cannot be determined by means of seismological studies [Di Toro et al., 2011,Di Toro et al., 2012].

This thesis aims at characterizing the architecture of the Foiana Fault Zone, hosted almost entirely in dolomitic-built rocks in the Southern Alps. **Section 2** describes the overall geological setting of the study area starting from a review of the current literature. **Section 3** describes the main structural features of the Foiana Fault Zone and neighbor areas by means of a remote sensing structural analysis (original data): the fault-fracture network is interpreted in a classical Riedel-type kinematic scheme. **Section 4** is dedicated to the field description (mostly original data) of the faults and fractures attitude and spacing, fault rock distribution, etc. of the fault zone. **Section 5** describes the microstructures (original data) found in the slip and damage zones of the FFZ. **Section 6** discusses the seismic origin of some of the microstructures (radial fractures, truncated grains, mirror-like surfaces, etc.) found in the fault zone rocks and the main factors (dragging of bedding surfaces, rupture directivity effects, role of confining stress, etc.) control the architecture of the FFZ.

Chapter 2

Geological setting

2.1 Area of study

The area of study was located in the north-eastern part of the Val di Non (Eastern Venetian Alps, to the west of the town of Bolzano, Fig.2.1a). The Dos de la Ceora is a NE trending 2 km long ridge, characterized (see section with satellite images, section 3) by the presence of regularly spaced and sub-parallel lineaments, interpreted as fault strands belonging to the Foiana Line [Cadrobbi, 1965]. To remark the aim of this study (i.e., the description of the architecture of a fault hosted in dolostone), and for consistency with the definition of faults in the current structural geology literature (faults are complex geological features including fault cores, damage zones, [Caine et al., 1996]), the Foiana Line [Cadrobbi, 1965, Prosser, 2000] is defined here as Foiana Fault Zone (FFZ). The studied location is easy to reach following the road (Via della Croce) from Castelfondo to the Laghetto della Regola.

At about 50 meters to the West of Dos de la Ceora, in a narrow V-shaped valley mostly covered by quaternary deposits, the FFZ is a sinistral transpressive fault which puts in contact the vulcanites of the Gruppo Vulcanico Atesino (Permian in age) to the W with the Sciliar Fm (Triassic in age) to the E. In this area, in the footwall the FFZ consists of a stack of sub-parallel fault strands, steeply dipping to N 135° and cutting the Sciliar Fm. The sub-parallel faults are considered as secondary faults of the main fault hosted in the western side of the valley. To describe the 3-D architecture and fault zone rock distribution of the FFZ, the fieldwork was carried on along the Via Della Croce (1) in an inactive cobble quarry, that allowed us to

produce a scan line roughly perpendicular to the sub-parallel fault strands and (2) in two large outcrops, sub-parallel to the sub-parallel fault strands and progressively closer to the main fault.

2.2   Regional geology

The Foiana Fault Zone plays a remarkable role in the evolution of the Southern Alps, as it is strictly related to the North Giudicarie Line, one of the most important faults of the Alps (a segment of the Periadriatic Line, PL, [Schmid et al., 1989]), and to the Trento-Cles Line, an important paleogeographic domain boundary and regional fault. But differently from the North Giudicarie line, the FFZ only involves the South-Alpine rocks, from the Variscan granodiorites of Monte Croce (crystalline basement) to the sedimentary covers of Tertiary age [Avanzini et al., 2007].

2.2.1   South-Alpine structural domains and deformation history

The South-Alpine structural domain is referred to the south verging (Africa verging) Alpine belt, separated by the Periadriatic Line from the north verging (Europe verging) Alpine-belt. With the exception of few and discontinuous exposures of the Variscan basement, most South-Alpine units consist of sedimentary covers of the Apulian plate, mostly pre-dating (Permian to Cretaceous) the Alpine orogeny (post-Cretaceous in age here [Prosser, 2000]). The Alps are the result of the collision of the Eurasian and the Adria (or Apula) plates. The main orogenic pulses that lead to the actual structure of the Alps are divided into eo-Alpine (subduction of the Ligurian-Piedmont Ocean: pre-collisional stage, Cretaceous to Eocene), meso-Alpine (collision of the Eurasian and Adria plates, Oligocene) and neo-Alpine (development of the south-verging thrust system in the Eastern Southern Alps: Miocene to today) [Doglioni and Bosellini, 1987].The rocks of the South-Alpine domain did not undergo to the alpine metamorphism, differently from the Alpine nappes north of Periadriatic Line [Dal Piaz, 1942].

The Africa- (or South-) verging Alpine chain can be divided in four main structural units listed as follows (in parentheses the age of activity [Castellarin and Can-
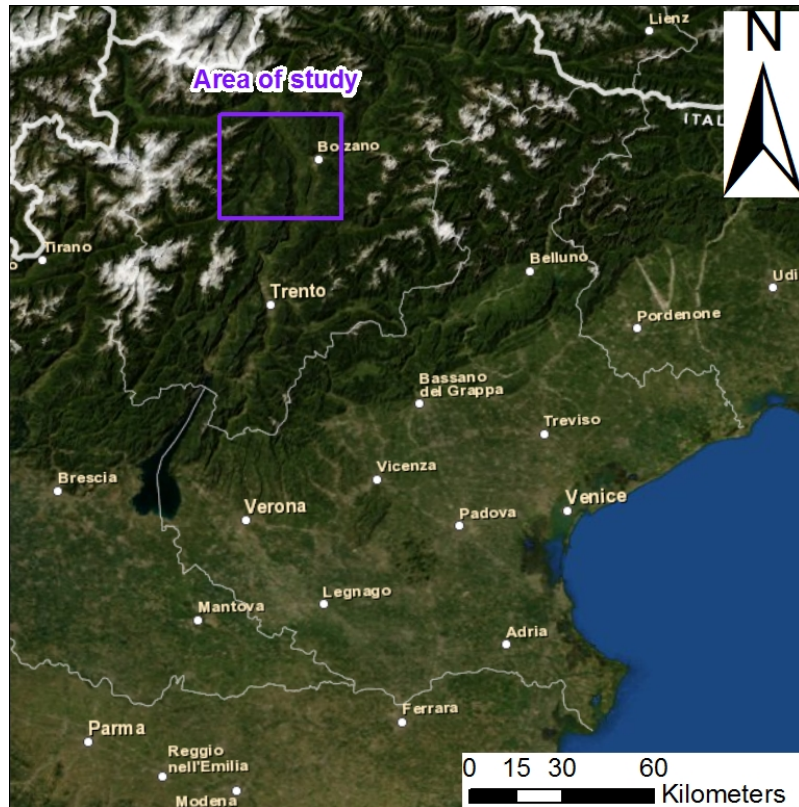
(a) Northeastern Italy
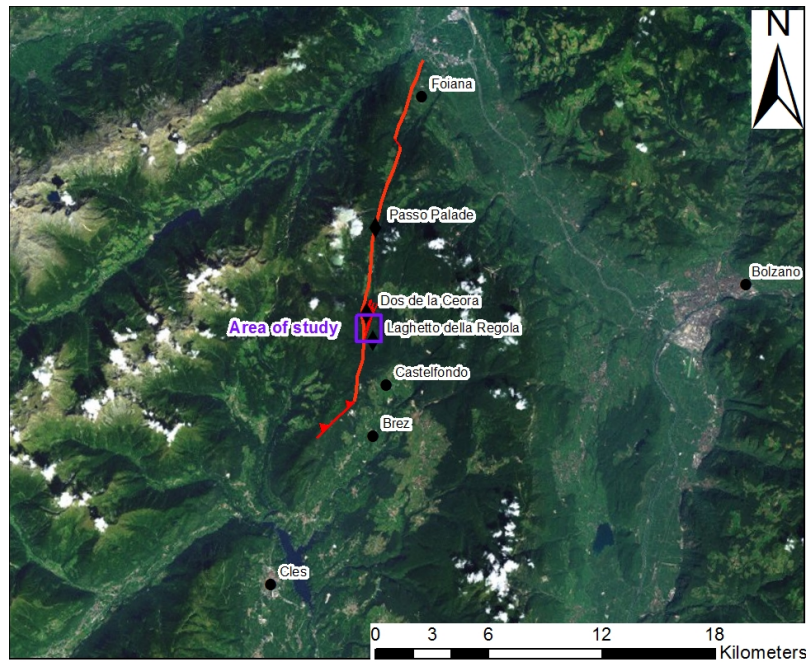
(b) Zoom in the study area

Fig. 2.1: Area of study: (a): North-east of Italy with area of study, (b): Zoomed with the Foiana Fault trace.

telli, 2000]):

- Pre-Adamello structural belt (Late Cretaceous-Early Eocene).

- Dinaric structural trends (two pulses: Eocene and Chattian-Burdigalian systems).

- Valsugana structural systems (Miocene: Serravallian-Tortonian).

- Bassano-Montello-Friuli structural belt (Messinian to Holocene).

In addition to the above structural units, we must include the Giudicarie belt, which underwent several deformative phases, often with reactivations, from the Valsugana (Serravallian-Tortonian) to the Adriatic (Messinian to Holocene) phase (Tab.2.1). This structural domain appears as an arc ranging from the Val Trompia thrust system into the South Giudicarie fault, involving the South-Alpine rocks in the surrounding area, W of the Trento-Cles line (Fig.2.2).
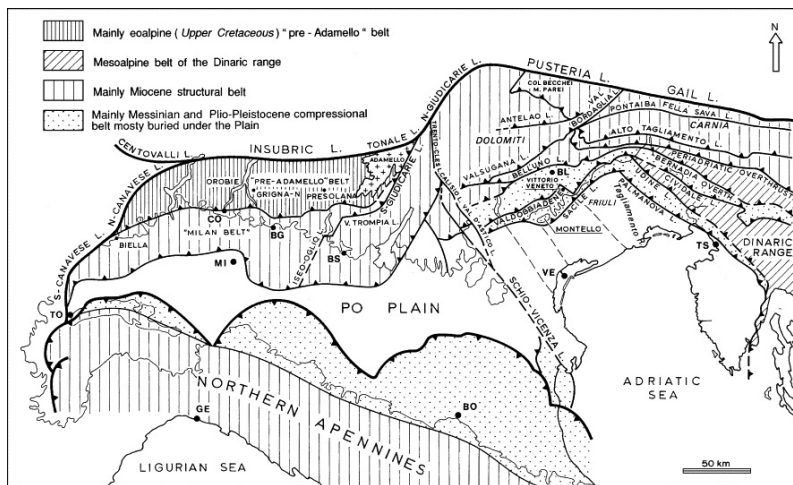

Fig. 2.2: Overview of the South-Alpine structural units [Castellarin et al., 2006].

The pre-Adamello structural belt is characterized, W of the Adamello and S to the Periadriatic Line, by S-verging ENE-WSW trending thrusts, which determined the shortening in the Orobic, Presolana and Grigna areas (Orobic Alps). This belt is called "pre-Adamello" because it predates the emplacement of the Adamello batholith (42 and 29 Ma). As a consequence, the activity of the Pre-Adamello structural belt is mostly Late Cretaceous to Early Eocene and records pre-collisional events (eo-alpine sensu [Doglioni and Bosellini, 1987]). There is no evidence of this

deformation event to the east of the South Giudicarie Fault (i.e., the area of study of this thesis).

Deformation phase	Age	Principal stress axis (azimuth)
Pre-Adamello	Late Cretaceous	
Dinaric	Eocene and Chattian-Burdigalian	N 26° and N 58°
Valsugana	Serravalian-Tortonian	N 340°
Adriatic	Messinian-Holocene	N 300° to N 330°

Tab. 2.1: Resume of the deformation phases in the Southern-Alps [Castellarin et al., 2006].

The Dinaric structural trends consist of two main orogenic pulses with similar orientation: Eocene and Oligo-Miocene (Chattian to Burdigalian). The Eocene activity was characterized by NW-SE trending thrusts with average N 58° compression direction (SW transport direction), which mostly affected the Alpi Giulie, Friuli and Carnia and Cadore and was concomitant to the meso-alpine collisional phase. These NW-SE trending structures were reactivated during the late Miocene Valsugana phase. Instead, the later Oligo-Miocene activity was characterized by WNW-ESE trending thrusts with N 26° compression direction (SSW transport direction), reactivation of Eocene thrusts and relation to the neo-Alpine Insubric or Elvetic compressional event. Both this phases are best developed instead in the eastern part of the South-Alpine, in Carnia and eastern Dolomites.

The Valsugana structural system is widely developed in the South-Alpine domain, and consists of E-W trending thrusts with average compression direction of N 340° (S transport direction) of Serravalian-Tortonian ages (late Miocene). The main structural feature is represented by the Valsugana thrust (about 20 km of horizontal shortening), which is linked to Giudicarie belt to the west by the Trento-Cles and Calisio-Valdastico N-S dextral transfer faults.

The Bassano-Montello-Friuli structural belt is the outer and younger part of South-Alpine chain, characterized by WSW-ENE trending and SSE verging thrust and fold geometries, Messinian to Holocene in age. The Schio-Vicenza and Valdalstico Lines transfer the deformations from the Eastern sector of the Southern Alps to the W, inside the Giudicarie belt structural domain.
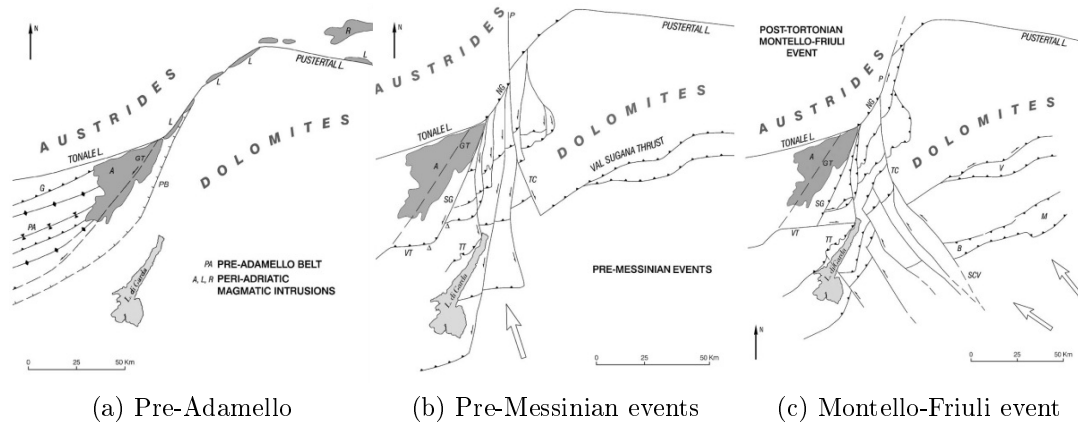
(a) Pre-Adamello   (b) Pre-Messinian events   (c) Montello-Friuli event

Fig. 2.3: Evolution of South-Alpine chain from pre-Adamello to Montello-Friuli event [Castellarin et al., 2006].

2.2.2 Structural setting of the studied area

In this section we review the literature on the FFZ and on the most important lineaments near the FFZ and discuss the kinematics and likely period of activity of the FFZ.

The North Giudicarie Fault System

The North Giudicarie Fault System (NGFS) which includes the North Giudicarie Fault (NGF) and the Merano-Mules faults (both segments of the Periadriatic Line) plus minor faults (Passeier or Passiria Fault, Jaufen or Giovo Fault, Foiana Fault Zone, Trento-Cles Line, etc.) located at the footwall and hangingwall of the NGF. The NGFS is composed of brittle faults and ductile shear zones [Viola et al., 2001]. During the neo-Alpine phase (Miocene) the overall activity of the NGFS was sinistral transpressive, allowing the overthrusting (S-SE transport direction) of the Australpine units over the South-Alpine sedimentary units. Prosser [Prosser, 2000] suggested strain partitioning in the NGFS between almost pure strike slip accommodated by the faults located in the footwall, including the FFZ (so in the Southern Alps), and almost pure thrusting accommodated by the NGF.

The NGF consists of two segments, divided at the locality of Proves (Fig.2.4). South of Proves, the NGF is mainly a thrust: the inner Australpine units override the South-Alpine sedimentary rocks. The fault zone includes tectonic lenses of South-Alpine sedimentary rocks. Here Oligocene in age sin-tectonic tonalites is exposed,
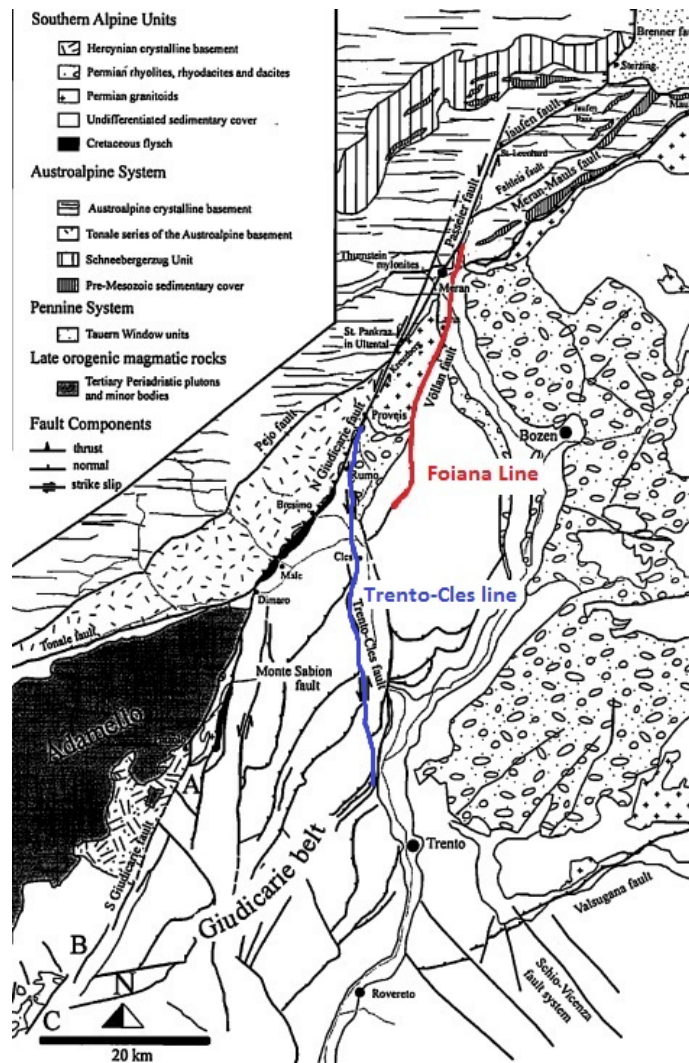
Fig. 2.4: Detail of the North (and South) Giudicarie Fault System and of the Giudicarie Belt (modified from [Viola et al., 2001]).

and outcrop again along the NGF North of Meran (near the Meran-Mauls line, [Viola et al., 2001]). The footwall of the NGF south of Proves is characterized by N-S trending strike slip faults (the FFZ, Trento-Cles) which are assumed to be active contemporary to the NGF during the Valsugana phase. The footwall faults reactivated Jurassic in age extensional faults. Also scattered outcrops of flysch are present, immediately in the footwall of the NGF. North of Proves, the dipping of the NGF becomes steeper and the kinematics is mainly strike slip [Viola et al., 2001].

About the other faults belonging to the NGFS, the Passeier Fault has a NNE-SSW trend (similar to the FFZ) and outcrops discontinuously in Passeier Valley, north of Meran. The fault dips steeply to the NW and accommodated a sinistral transpression. Fault activity was probably contemporaneous to the activity along the NGF (north of Proves). The Meran-Mauls fault, segment of the Periadriatic Line, is NE-SW trending, and represents the tectonic boundary between the Australpine and the Variscan South-Alpine basement. The Meran-Mauls fault is similar to the southern segment of the NGF in terms of geometry and structural evolution, with thrusting transport direction to SE.

The Foiana Fault Zone

The Foiana Fault Zone is one of the about N-S striking faults cutting the NGF footwall (the other being the Trento-Cles Line described in section 2.2.2). The FFZ is a steeply dipping transpressive sinistral fault, with average strike NNE-SSW, sub-parallel and located 4-5 km to the east of the NGF. North of Passo Palade the FFZ puts in contact the metamorphic South-Alpine basement to the W with the Mesozoic covers to the E. To the south of the village of Foiana and 3 km W of Tesimo, a left step-over of the FFZ is suggested by the presence of a sinistral transfer fault [Avanzini et al., 2007], but hidden beneath glacial sediments. South of Passo Palade the contact is between Permian volcanics (Gruppo Vulcanico Atesino) to the W and the Werfen (silicoclastic and carbonatic) Formation (Late Permian- Lower Triassic) to the E. In the footwall of the fault zone, secondary faults are arranged in sub-parallel strands, which can be followed until the Dos de la Ceora locality.

The fault strands seem to continue also in the hangingwall (Permian volcanics and volcanoclastics) of the FFZ between Dos de la Ceora and Castelfondo localities.
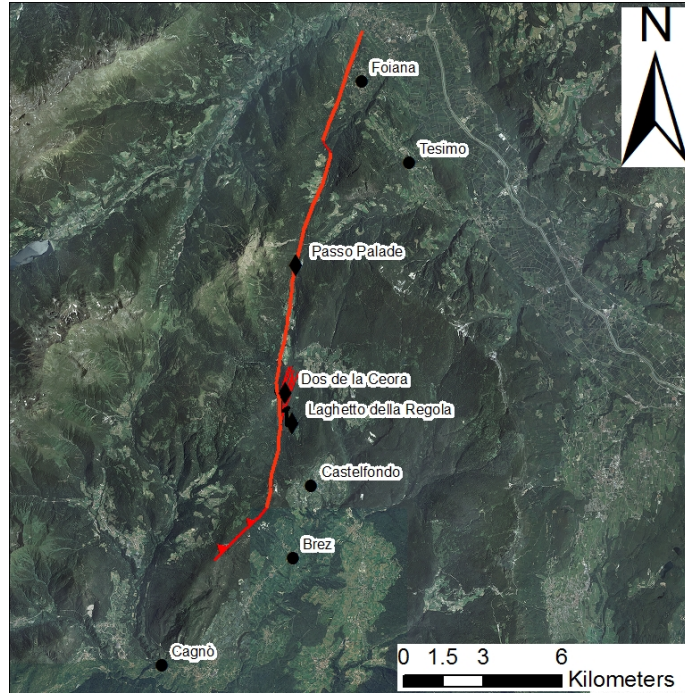
Fig. 2.5: The Foiana Fault Zone main trace, from Appiano Map [Avanzini et al., 2007].

SW of the village of Castelfondo, the FFZ bends from NNE-SSW to NE-SW and its dip decreases from average 80° to 50°. This fault bend corresponds to the presence, in the FFZ footwall, of a 300 m thick cataclastic zone (including pulverized rocks, section 4.1), on which badlands morphology develops. Here the FFZ hangingwall forms a fault-propagation fold (anticline) and merges, to the SW, into the Trento-Cles Line (TCL): the fault-propagation anticline includes the entire NE-SW trending ridge near the village of Cagnò. In the footwall of the FFZ and to the E of the hangingwall anticline, a kilometre-in-scale gentle in curvature drag syncline occupies the Val di Non to the North of the S. Giustina Lake and just SE of Cagnò (not shown in Fig.2.5). From north to the south the calculated vertical throw using Appiano map along the FFZ decreases from 1100 to 300 meters.

The Trento Cles Line

The Trento-Cles Line (TCL) is the other important regional lineament of the NGFS. The TCL strikes about N-S and, similarly to the FFZ accommodated sinistral strike slip during the Valsugana phase. North of the locality of Rumo, the TCL strikes NNE-SSW for 2-3 kilometres and then merges into the NGF (Fig.2.4). The TCL

activity was relevant during the Late Triassic to Early Jurassic per-Alpine extension, as it separates the Brenta Units from the Val di Non units, the latter located to the east of the TCL (see Fig.2.6 and discussion in next section 2.2.3).The original geometries of the TCL are in part obliterated by the Neogene reactivation (sinistral strike slip overprinting), compatible with a N 340° shortening (principal horizontal stress direction).

2.2.3   Stratigraphy of the area

The stratigraphic succession around the FFZ belongs to the Val di Non unit, which corresponds to the paleo-geographic Triassic-Jurassic domain to the east of the TCL (Fig.2.6). This paleo-domain underwent (1) smaller subsidence with respect to the paleo-domain west of the TLC (i.e., Brenta Unit) during the Triassic and, (2) almost absence of sedimentation and emersion during the Early Jurassic. This is suggested, in the Val di Non Unit, by the limited thickness (1) of the Dolomia Principale Fm (i.e., the thickness decreases from the 1200 m in the Dolomites s.s. to 300 m here) and, (2) of the lower Jurassic sedimentary units. Here, the Jurassic to Cretaceous in age Rosso Ammonitico Veronese Fm. and Scaglia Rossa Fm. are in contact with the Dolomia Principale Fm.: the Early Jurassic Calcari Grigi Group is absent (in the area the occurrence of the Calcari Grigi is only documented along few tectonic slices parallel to NGF). Instead, in the Brenta unit (west of the TLC), the Dolomia Principale (Late Triassic) succession is thicker and the Calcari Grigi group (Early Jurassic) present. These stratigraphic evidences are indicative of the sin-sedimentary Late Triassic to Early Jurassic activity of the TCL.

In the following paragraphs we provide a short description of the entire sedimentary succession outcropping in the Appiano geological map (Fig.2.7). The formations deformed by the FFZ will be further discussed in section 4.1.

Metamorphic basement

The Bressanone unit outcrops in an area comprised between the NGF and the FFZ, W of Foiana village. It is a low grade Variscan metamorphic unit intruded by Permian plutons.
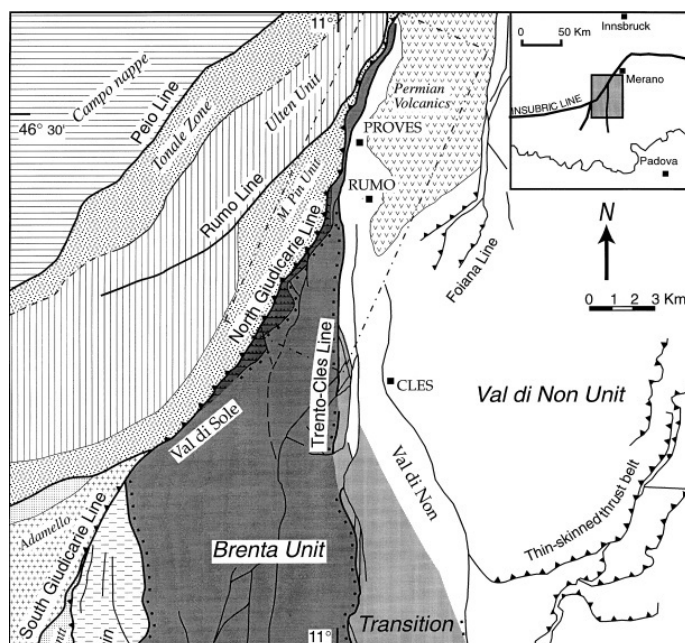
Fig. 2.6: The paleogeographic domains around the study area [Prosser, 2000]

Permian magmatic event

The Permian magmatic event is widespread in all the area, strongly connected to postorogenic extension activity [Bargossi et al., 2004]. It includes intrusive rocks and volcanics and vulcanoclastic rocks. The Monte Croce Granodiorite outcrops between FFZ and NGF north of Proves, and the intrusive contact with the metamorphic basement is preserved to the S (locally outlined by the development of cornubianites over basement phyllites), while the other contacts are tectonic.

The Gruppo Vulcanico Atesino (GVA) represents an important stratigraphic succession (in some areas 2000 m thick) which consist predominantly in pyroclastic flow deposits, linked to fissural volcanic emissions in continental environment, intercalated with many vulcanoclastic deposits (mainly deposited during the pause in volcanic activity). The lower limit is an unconformity above the crystalline basement and the upper one another unconformity with the Arenarie di Val Gardena Fm. Inside the GVA are of particular interest, because of the outcropping in our study area, the Monte Luco and the Tregiovo Formations. The Monte Luco Fm. is well recognizable by remote sensing (LIDAR DEM) because of the prominent domes and lava flows which accumulated over up to 1300 m of volcanic succession. The most important outcrop is in the tectonic slice between NGF and FFZ, south of

Proves, near Monte Luco. The Tregiovo Fm. was interpreted as the filling of intra-volcanic basins, generated by pull apart along NE trending dextral strike slip faults (Permian age). Correlation with Collio and Tione units, belonging to the Brenta and Lombardy domains are found . The outcrops are in the Tregiovo village area, between the NGF and FL.

Permian to Cenozoic sedimentary cover

The sedimentary cover in the study area ranges from Permian to Eocene deposits: here will be described the most relevant Formations (Fig.2.7).
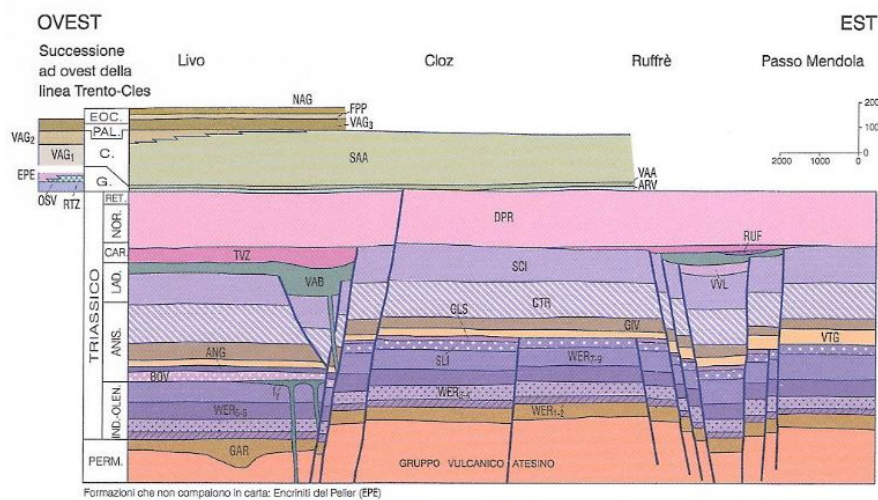

Fig. 2.7: Permian to Cenozoic sedimentary cover. AVG Arenaria della Val Gardena; WER Werfen Fm; SLI Dolomia del Serla Inferiore; BOV Carniola di Bovegno; ANG Calcare di Angolo; GLS Gracilis Fm; VTG Voltago Cgm; GIV Giovo Fm; CTR Contrin Fm; SCI Sciliar Fm; VVL Calcare della Val Vela; VAB Vulcaniti Basaltiche; RUF Ruffrè Cgm; TVZ Travenanzes Fm; DPR Dolomia Principale; ARV Rosso Ammonitico Veronese; VAA Scaglia Variegata Alpina; SAA Scaglia rossa; VAG Val d'Agola Fm; FPP Ponte Più Fm; NAG Calcare di Nago [Avanzini et al., 2007].

- Arenaria della Val Gardena. Terrigenous sandstones and conglomerates with caliches. The lower limit is para-concordant over the Gruppo Vulcanico Atesino rocks. The Arenarie della Val Gardena result from the erosion in an arid sub-aerial continental environment of the GVA and their deposition in alluvial plains (Late Permian).

- Werfen Fm. Succession of carbonate, terrigenous and mixed rocks, deposited in a marginal sea environment (Late Permian to Olenekian, Early Triassic).

24

- Dolomia Del Serla Inferiore. Dolostone and evaporite rock layers. The Formation deposited in a tidal flat under high evaporation conditions and is etheropic to the Carniola di Bovegno, which outcrops in the study area only W of the FFZ. The Carniola di Bovegno Fm. consists of dolostones layers alternated with evaporite layers, probably indicating a sabkha environment with intertidal to subtidal conditions. It is a typical unit widespread in Lombardy area (Late Olenekian to Early Anisian).

- Calcare di Angolo. Dolostones and calcarenites with fossils and ripples, representing prevailing carbonate deposition over terrigenous, indicating subtidal bay conditions (Early to Middle Anisian).

- Gracilis Fm. Alternating dolostones and calcarenites, indicating similar conditions to Calcare di Angolo. Etheropic to the previous formation, it results from sedimentation in small tidal flats, located in carbonate platforms with ingression of terrigenous sediments (Early to Middle Anisian).

- Voltago Conglomerate. It is a terrigenous horizon, indicating continental depositional environment, trending to the top to tidal flat conditions (Middle Anisian). It marks the onset of the first important Anisic sequence.

- Giovo Fm. Clastic and carbonate sediments, deposited in marginal sea environment. It is articulated in 3 members and embraces the second Anisian sequence and the beginning of the third (Middle Anisian).

- Contrin Fm. Already defined as part of Mendola Fm, subtidal member (in the PAT cartography), consists in subtidal dolostones, representing carbonate platform in subtidal conditions (Late Anisian). The upper contact is often erosional marking a partial emersion of the rocks due to sinsedimentary tectonics.

- Sciliar Fm. Dolostones with peritidal cycles, representing an aggradating carbonate platform, bounded by subsiding basins and characterized by emersion in some sectors. The lower limit with the Contrin Fm. is marked by a tepee horizon and the upper limit varies from paleokarst surfaces to paraconcordance with Vulcaniti basaltiche (Late Anisian to Ladinian).

- Calcare della Val Vela. Stratified dark limestones with chert nodules and increasing terrigenous component to the top. Indicates intra-platform environments, filled progressively by terrigenous sediments and capped by Vulcaniti basaltiche. (Ladinian)

- Vulcaniti basaltiche. Volcanic complex made of basaltic lava flows often evolving into lava breccias, indicating subaerial weathering and erosion (Late Ladinian). They mark the very documented and important Ladinian volcanic event, widespread in the Dolomites area, where they form dykes cutting the older formations.

- Ruffrè Conglomerate. Conglomerate built prevalently of volcanics clasts and dolomitic matrix, erosive limit over Vulcaniti basaltiche or Calcare della Val Vela (Late Ladinian). It indicates the erosion of volcanic and carbonate rocks in subaerial environment.

- Travenanzes Fm. Dolostone and pelitic intercalations, indicating continental to lagunar and evaporitic environment. The upper limit to Dolomia Principale is transitional. (Carnian)

- Dolomia Principale. Dolostone organized in metric peritidal cycles, indicating a wide carbonate platform with dominating tidal flat facies (Late Carnian to Norian).

- Calcari Grigi Group. In the study area they are only represented by the Rotzo Fm and the Oolite di S. Vigilio Fm., both indicating tidal flats at the Piattaforma Trentina margin. The Group outcrops only along the NGF tectonic slices (Early Jurassic).

- Rosso Ammonitico Veronese. The lower limit is often on the Dolomia Principale, higlighted by a hardground horizon. It represents hemipelagic environment with widespread sedimentary condensation, over a structural high (drowning of Piattaforma Trentina). (Middle to Late Jurassic)

- Scaglia Variegata Alpina. This formation is made by micritic limestones with intercalated marls, and some black shales indicating anoxic conditions. At

the base the Maiolica Fm is recorded only locally and sometimes the contact is sharp over the Dolomia Principale, the upper limit is transitional with increasing terrigenous input. Indicates hemipelagic basins with little water circulation. (Late Jurassic to Early Cretaceous)

- Scaglia Rossa. Limestones with variable marl percentage. Hemipelagic deposition with strong input of terrigenous sediments from the north. (Late Cretaceous to Paleocene)

- Val d'Agola Fm. Terrigenous sedimentary succession contemporary to the pre-Adamello deformation phase, eo-alpine. Corresponds to the Lombardy flysch (Late Cretaceous to Middle Eocene).

- Ponte Pià Fm. Calcilutites to Nummulites calcarenites indicating basinal sedimentation near carbonate platforms. (Early to Middle Eocene)

- Calcare di Nago. Nummulites limestones and micritic limestones indicating carbonate subtidal platform in shallow water conditions. (Middle to Late Eocene).

Chapter 3

Architecture of the Foiana Fault Zone from remote sensing structural analysis

3.1 Introduction and methods

The thesis aims at describing the architecture (fault rock distribution, type of fault rocks, etc.) of the Foiana Fault Zone at different scales, from remote sensing to field survey and microstructural analysis of the fault rocks. Detailed field and microstructural studies focused on the outcrops of the Doss de la Ceora (section 4), whereas a remote sensing structural analysis was performed along the entire trace of the FFZ from southwest of Merano to northeast of Cles. The lineaments associated to the FFZ were interpreted using the Riedel nomenclature [Riedel, 1929] with the aim to constrain the kinematics of the Foiana Fault Zone at the regional scale.

The remote sensing structural analysis was carried out on orthorectified aerial photographs and hillshade images extracted from LIDAR-based (Light Detection and Ranging) digital elevation models (DEMs) over an area of about 30 km^2. The aerial photographs and the DEMs were downloaded from the websites of the Trento and Bolzano provinces or obtained from the local offices. The orthorectified aerial photographs had a spatial resolution of 0.5 m, while the LIDAR-DEMs had a spatial resolution of 1 m for the Trento province and 2.5 m for the Bolzano province. The hillshade images were generated from the DEMs with different illumination angles
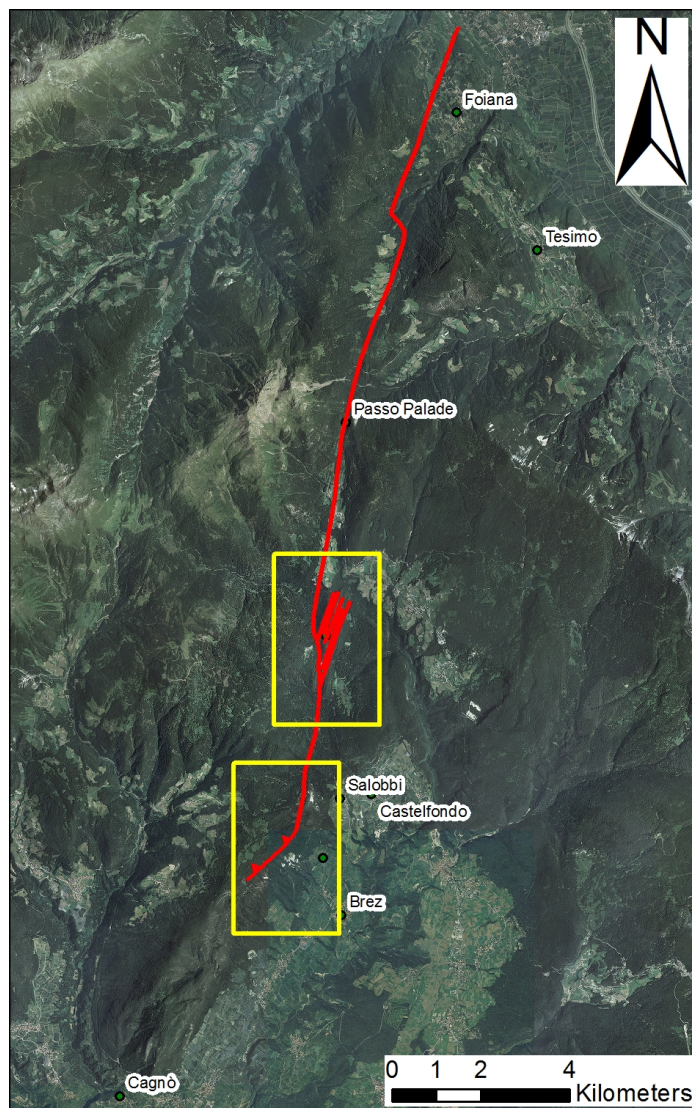
Fig. 3.1: Overview of the whole Foiana Line trace. Yellow rectangles indicate the areas studied in Fig.3.4.

(i.e. 45°, 135°, 225°, 315° from the azimuth and 45° of inclination) using the software ArcGis 10 (Fig.3.2).
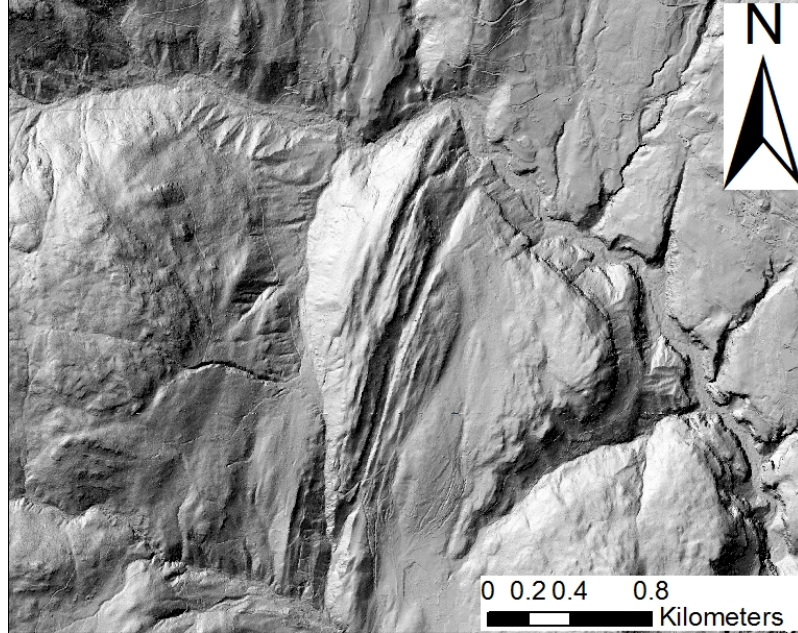

Fig. 3.2: Example of a hillshade image (illumination angle of N 315° from the azimuth and 45° of inclination) of the Doss de la Ceora locality. Here the stack of sub-parallel fault strands related to the FFZ has a prominent topographical expression with ridges and trenches.

The combination of aerial photographs, hillshade images and published geological maps [Avanzini et al., 2007] allowed to recognize the main lineaments of the area, which were drawn using the software ArcGis 10. The outlined lineaments comprised faults, joints, bedding and foliation surfaces. For instance many of the lineaments cutting volcanic rocks (the GVA, see section 2.2.3) were joints (i.e. cooling joints), whereas many of the lineaments affecting basement metamorphic rocks and sedimentary covers corresponded to foliation and bedding surfaces respectively. Nevertheless most of the drawn features were classified as general lineaments because it was not possible to verify their origin in the field. The average strike of each lineament was calculated using an ArcGis 10 script and the resulting strike dataset was represented by using rose diagrams (Openstereo software [Grohmann and Campanha, 2010]). Moreover the lineaments were organized within eight intervals of strike, 22.5° each, and classified according to the Riedel nomenclature.

3.2 Results

The FFZ trace was often difficult to be recognized in the hillshade images and aerial photographs, therefore the fault trace was largely extrapolated from the published geological maps [Avanzini et al., 2007]. A significant exception was the area to the north of Castelfondo at the Doss de la Ceora, where the FFZ marks the lithological contact between the volcanics and plutonic massive rocks to the west and the stratified sedimentary rocks to the east, which is characterized by a prominent morphological expression. So it was possible to map with high precision the lineaments associated to the Foiana Fault Zone at the Doss de la Ceora. This fault zone section will be described in detail in section 4.

The average strike of the Foiana Fault Zone is NNE-SSW, but in its southern sectors (south of the village of Castelfondo) the FFZ bends to NE-SW (Fig.3.1 and 3.3). The lineaments around the trace of the FFZ (within 2 km from the fault zone axis) were interpreted as secondary faults of the Foiana system. Moving from the south to the north along the FFZ (for about 30 km), four fault sets with different strike (indicated as the angle from the azimuth) were recognized (Fig.3.3 - rose diagram):

- N 20° striking set;

- N 135° to N 160° striking set;

- N 70° striking set;

- N 120° striking set.

This pattern of secondary faults can be interpreted by applying the Riedel classification of the shear fractures related to a major fault. Considering a major fault striking N 20°, as the average strike of the FFZ; the N 20° striking fault set can be interpreted as a Y-shear fracture set, the N 135° to N 160° striking fault set can be interpreted as a R-shear fracture set, and the N 120° and N 70° striking fault sets as R' and X shear fracture sets respectively. This network of secondary faults is coherent with a far-field stress tensor characterized by a principal compressive axis striking N 340° (i.e. Valsugana deformation phase), leading to a sinistral transpressive kinematics along the Foiana Fault Zone. The orientation of the lineaments
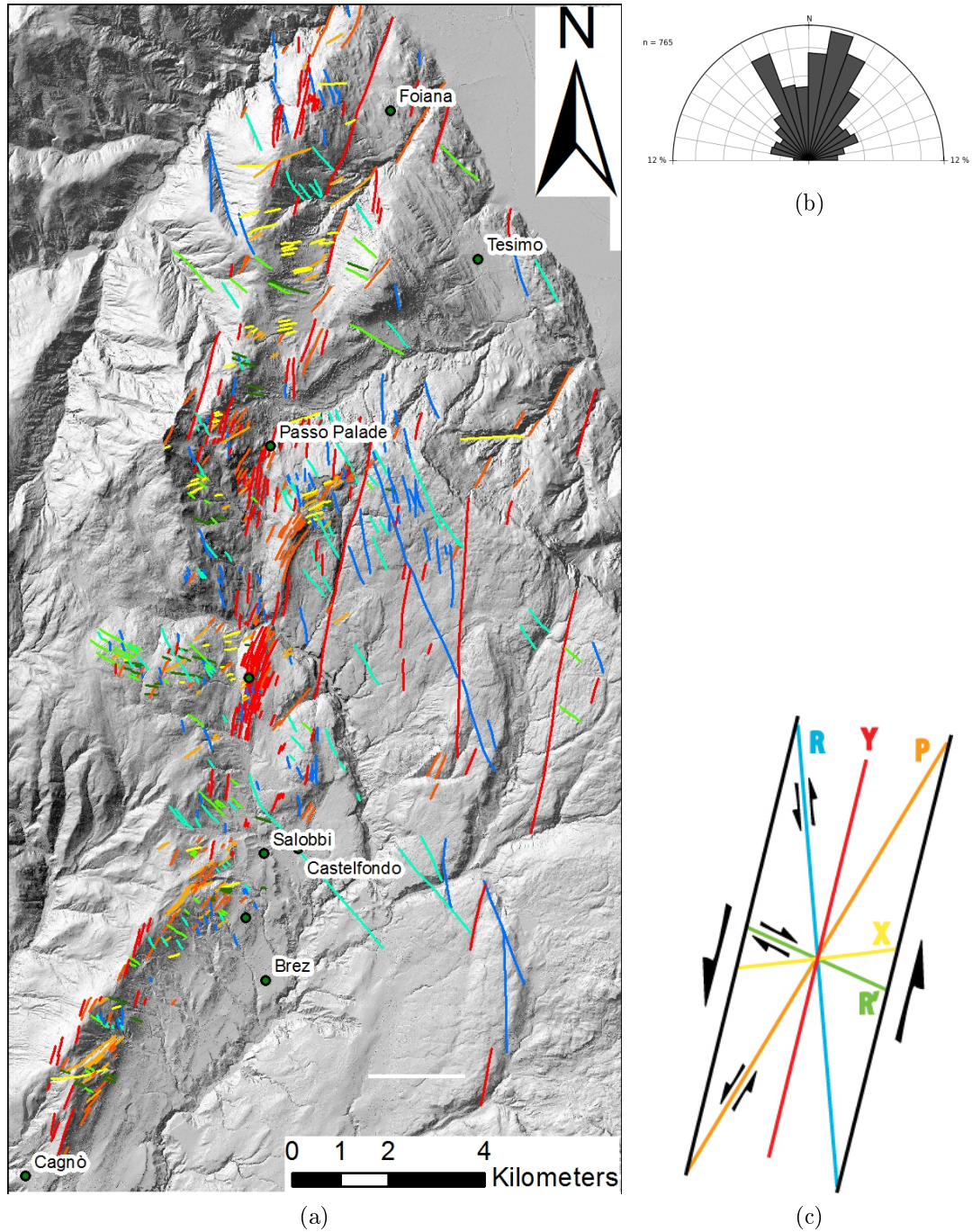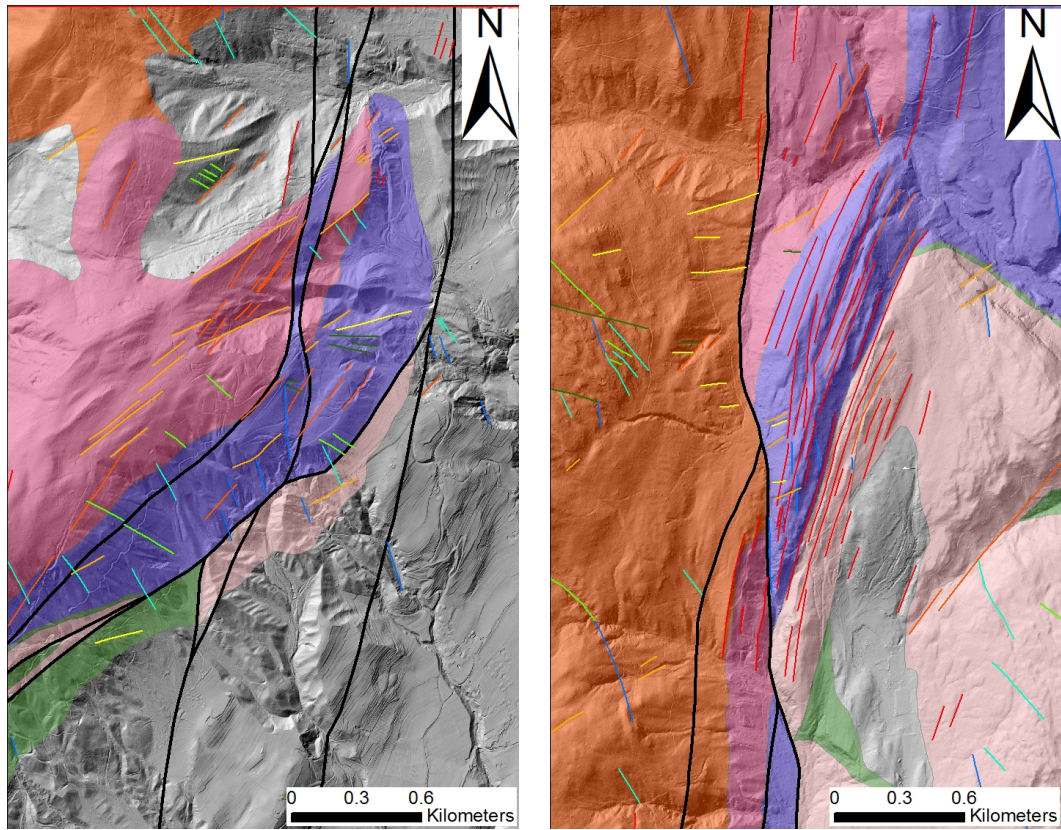
Fig. 3.3: Remote sensing structural analysis along the FFZ. (a) Map of the linea-
ments around the FFZ and interpretation according to the Riedel scheme of shear
fractures (section (c) of the figure). Red lines indicate the N 20° set, interpreted
as Y-shear fractures; light blue and blue lines the indicate the N 135° to N 160°
set, interpreted as R-shear fractures; light green lines indicate the N 110° set, inter-
preted as R'-shear fractures, and yellow lines the N 70° set, interpreted as X-shear
fractures. (b) Rose diagram with frequency-strike distribution of the lineaments
around the FFZ. The dominant set of lineaments is the N20° striking, parallel to
the average strike of the FFZ. (c) Riedel scheme for the classification of secondary
shear fractures related to a major fault.

around the FFZ is also strongly affected by the changes of strike characterizing the FFZ moving from the south to the north, as evidenced from the following comparison in Fig.3.4.
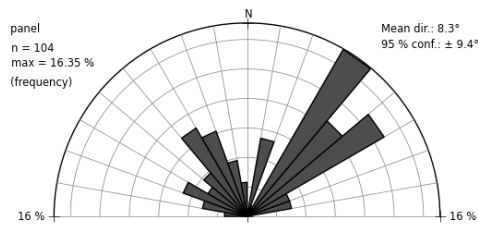
In the southern sector of FFZ (to the East of Carnalez), approaching to the fault bend, the strikes of the lineaments are scattered in several sets with various orientation. Nevertheless a dominant lineament strike of N 40-50°, consistent with the strike of the FFZ bend, is recognizable (see Fig.3.4a). The lineaments were drawn mainly in the hangingwall block, as the footwall block of the fault is hidden under quaternary deposits. Both the footwall and hangingwall blocks consist of sedimentary rocks from the permo-cenozoic covers.

At the Doss de la Ceora locality, which is studied in detail in this thesis, the dominant set of lineaments strikes N 20° and is consistent with the strike of the FFZ (see section 4). This set of lineaments correspond to a stack of sub-parallel fault strands with spacing of 30-50 m. Few kilometers north of the Doss de la Ceora the stack of faults bends to the N 45° into a largely fractured area. In general the lineaments related to the FFZ were well recognizable in the footwall block of the fault, which consists of the dolostones of the Sciliar Formation. On the contrary the hangingwall block of FFZ, which consists of volcanic rocks, is affected by lineaments striking from N 85-90° to N 100-120°, interpreted as cooling joints of the volcanic host rock. To the north of the Doss de la Ceora the lineaments follow the dominant strike of N 20°, parallel to the average strike of the FFZ.
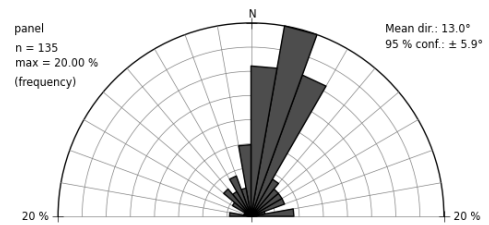
(a) Carnalez   (c) Doss de la Ceora

(b)   (d)

Gruppo Vulcanico Atesino   Sciliar Dolostone

Arenaria Val Gardena Fm.   Dolomia Principale Fm.

Lower Triassic rocks   Jurassic to Cretaceous rocks

(e)

Fig. 3.4: Relationships between lineament orientation and strike of the FFZ, in the yellow-boxed areas of Fig.3.1. The black lines indicate the main strands of the Foiana Line according to the Appiano Geological map [Avanzini et al., 2007]. (a) Zoom at the FFZ bend: the strikes of the lineaments are scattered (see rose diagram, (b)). The dominant strike is NE-SW consistent with the fault bend. (c) Zoom at the Doss de la Ceora: the strikes of the lineaments are clustered in the interval N 0-20° (see rose diagram, (d)). (e) Simplified geology of the FFZ, see section 2.2.3 for formation names. Colors of the lineaments are the same of Fig.3.3.

Chapter 4

Architecture of the Foiana Fault Zone from field geological survey

4.1 Introduction and methods

In this section I describe how the architecture of the Foiana Fault Zone evolves along strike from south to north in terms of fault geometry, dominant sense of shear and type and abundance of fault zone rocks.

The architecture (i.e., geometry and fault rock distribution) of the FFZ was described at three outcrops (outcrops 1-3), which from the south to the north were distributed over a length of 6 km along fault strike (Fig.4.1). The outcrops were:

1. Outcrop (1) located to the west of the village of Carnalez, in correspondence to the NE-SW oriented FFZ restraining bend. Here the FFZ consisted of 300 m thick zone of intensely fragmented dolostones resulting in badlands morphology, and displayed a dominant reverse kinematics.

2. Outcrop (2) located to the west of the village of Salobbi, along the road from Salobbi to Lauregno. The outcrop was just to the north of the FFZ restraining bend where the FFZ strikes about N-S. The fault zone was 200 m thick and consisted of intensely fragmented dolostones cut by faults with scattered attitudes and highly reflective (mirror-like) fault surfaces.

3. Outcrop (3) located at the locality of Doss de la Ceora, where the FFZ strikes from N-S to NNE-SSW. Here the fault zone was 200 m thick and consisted of
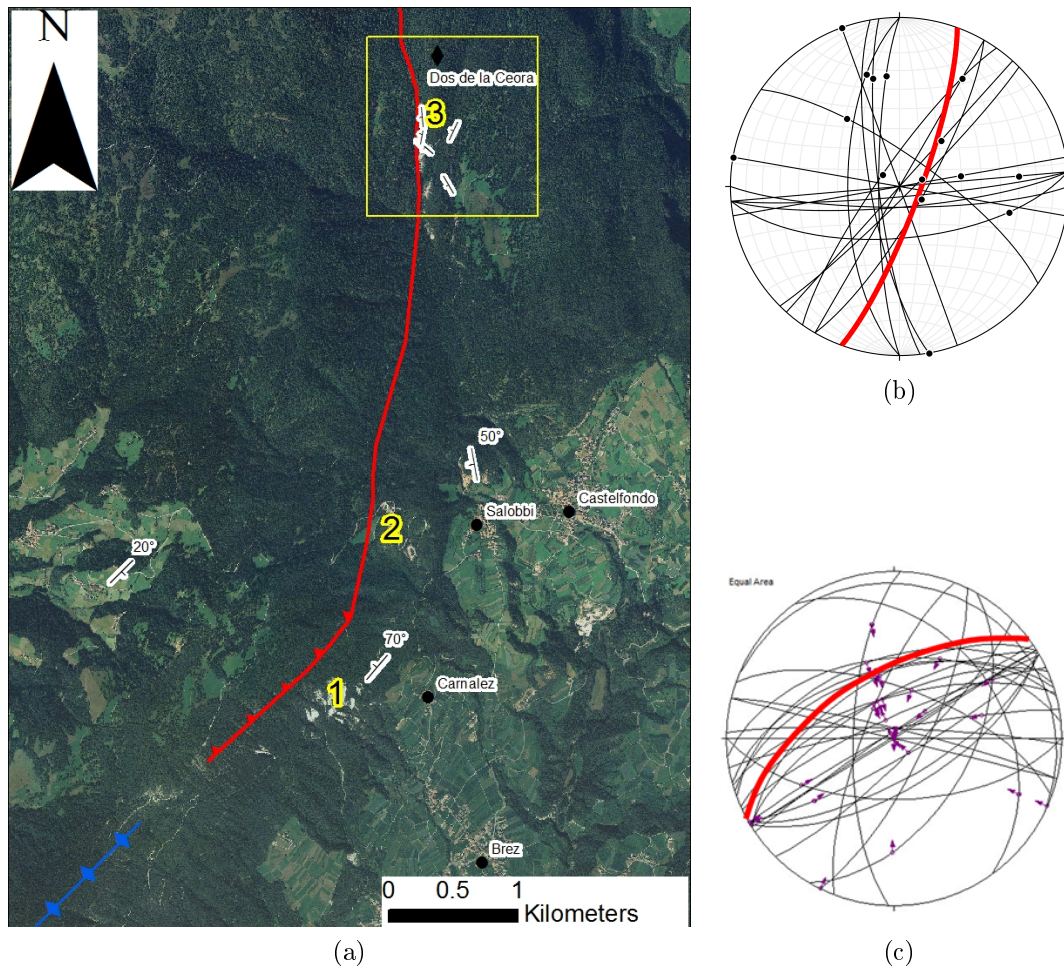
(a)

(b)

(c)

Fig. 4.1: (a) Overview of the southern sector of the Foiana Fault Zone. Numbers indicate the outcrops of the FFZ described in this section. Bedding attitudes are derived from the Appiano geological map [Avanzini et al., 2007]. The square highlights the Doss de la Ceora area, which was studied in detail in this thesis. (b) Stereographic projection of the structural data from Doss de la Ceora (outcrop 3 in (a)); (c) Stereographic projection of the structural data (outcrops 1 and 2 in (a)). By comparing (c) with (b) it is evident the change in strike and kinematics of the faults moving from south (mainly dip-slip) to the north (mainly strike-slip). Data of stereoplot (c) from Michele Fondriest.

intensely fragmented ("pulverized") dolostones cut by a stack of sub-parallel, almost sub-vertical fault strands with dominant strike-slip kinematics. Some of these faults were characterized by polished to mirror-like fault surfaces.

For each outcrop, I present below the structural data (attitude of faults and fractures, and where possible, their sense of shear) collected along oriented scan lines or at structural stations with known geographical position (i.e. GPS coordinates), and the fault zone rock types.

I performed most of the field work in outcrop (3) and in collaboration with Michele Fondriest. I will give more space here to the data I collected. Nevertheless to discuss the internal structure of the FFZ and how it evolves along fault strike, I will also include a summary of the data collected in outcrops (1) and (2) by Michele Fondriest [Fondriest et al., 2012, Di Toro et al., 2012].

In outcrop (3), the FFZ is hosted in the dolostones of the Sciliar Formation. These sedimentary rocks were organized in peritidal cycles up to 0.6-1 m thick with stromatolitic laminations and trails of fenestrae (Fig.4.2). The top of the peritidal cycles was marked by up to few centimeters thick pelitic to marly horizons. Locally anastomosing paleosoils and paleokarst deposits were also documented. Within this cyclic organization of protolith rocks, some darker, greyish rocks are documented, named here as "greyish facies dolostones".

The rocks building the Foiana Fault Zone were affected by intense and pervasive fragmentation. These fault rocks had the following characteristics which suggest that they have been shattered *in situ*: (i) the primary sedimentary structures of the host rock (i.e. Sciliar Fm.) such as intercalations of marly dolostones parallel to the bedding and the stromatolitic laminations were preserved and recognizable (not obliterated by fracturing); (ii) there is no evidence of significant shear strain; (iii) the rocks are pervasively fractured (extension-type fractures) from the meso- to the microscale. Some of these characteristics are typical of pulverized rocks, a type of fault rock frequently interpreted as the product of dynamic shock loading during the passage of seismic ruptures [Brune, 2001, Dor et al., 2006]. The mechanism of formation of the shattered dolostones will be discussed in section 6.

The shattered dolostones of the FFZ were described and mapped in the field using an expeditious ad hoc-designed classification (see Tab.4.1). Basing on the average

size of the rock fragments, the shattered dolostones were distinguished between:

- Fragmented dolostone: the average rock fragment size (d) was larger than 3 cm. Brittle deformation was accommodated by extensional fractures (joints). Four or five sets of joints were present.

- Highly fragmented dolostone: the average rock fragment size (d) was between 0.1 cm and 3 cm. This type of fault rock was often outcropping within small erosive gullies and was cut through by the sub-parallel fault strands.

Many of the faults cutting through the shattered dolostones were characterized by strong shear strain localization next to polished to mirror-like slip surfaces.

Fig. 4.2: The host rock: dolostone of the Sciliar formation. The stromatolites laminations and the trails of fenestrae typical of this rock define the attitude of the bedding and allow to distinguish in several exposures newly formed fracture surfaces (tectonic, unloading, etc.) from the bedding surfaces.

Class name	Average rock fragment size (cm)
HF Highly fragmented	$0.1 < d < 3$
F Fragmented	$d > 3$

Tab. 4.1: Classes of rock damage recognized in the field
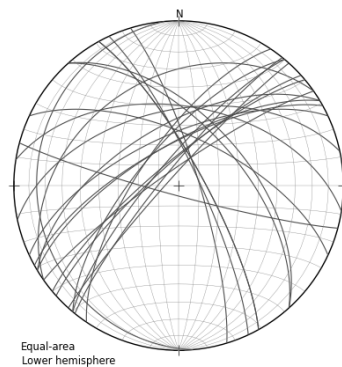
(a) Fragmented rocks
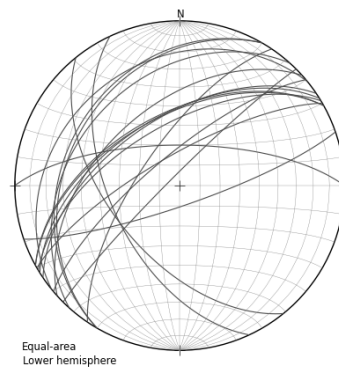

(b) Highly fragmented rocks

Fig. 4.3: Appearance of the fault rocks in the field

(a) The outcrop 1, NW-SE section

(b)

(c)

Fig. 4.4: Outcrop 1. (a) The overturned bedding of the Sciliar Fm. is exploited by the ENE-WSW striking faults. (b) Stereoplot (equal area) of the fault planes. (c) Stereoplot (equal area) of the bedding (from Michele Fondriest).

4.2 Architecture of the FFZ from Carnalez to Doss de la Ceora

4.2.1 Outcrop 1: 500 m to the W of the village of Carnalez

Fault geometry, kinematics and preexisting structures

The most evident geometrical feature of the southern sector of the FFZ was the NE-SW trending bend to the west of the village of Carnalez (Fig.4.1). The fault bend was located at the southern tip of the FFZ, which just to the south faded into a NE-SW trending fault propagation anticline (see section 3.2). The anticline morphologically represented the western flank of the Mt. Ozol down to the S. Giustina lake (Fig.2.4) and was highlighted by the overturning of the sedimentary covers, including the dolostones of the Sciliar Fm.. The FFZ cut through the eastern limb of the anticline giving rise to an area of ca. 0.2 x 0.3 km^2 characterized by badlands morphology. The average dip direction of the FFZ was N 310-320° with dip angles in the range 50-70° and dip-slip reverse kinematics. The estimated cumulative vertical throw across this section of the fault zone was ca. 0.3 km (vertical separation calculated from Appiano geological map) and was accommodated by a lot of tens to hundreds of meters in length secondary faults mainly dipping N 300-340° with dip angles in the range 40-80° (see Fig.4.4b). The attitude of this set of faults was consistent with that of the bedding which was verticalised to overturned. Therefore many of the faults within the FFZ exploited the bedding as preexisting structure (Fig.4.5 and 4.4).

Fault zone rocks

At outcrop (1) the FFZ was ca. 300 m thick and consisted of 10-40 m thick bands of highly fragmented dolostones alternated to up to 10 m thick bands and lenses of fragmented dolostones (see Fig.4.4). The contact between fragmented and highly fragmented dolostones was mainly represented by the N 300-340° dipping faults, suggesting a fault zone structure characterized by alternated sub-parallel fault rock bands with different intensity of damage. It was difficult to recognize the main fault trace both from remote sensing analysis (section 3.2) and from the field survey.

The most recent geological map of the area [Avanzini et al., 2007] interpreted the zone of shattered dolostones (fragmented and highly fragmented) as belonging to the footwall of the FFZ. Although the FFZ was exposed over a wide area within outcrop (1), large parts of the outcrop (especially in correspondence to the highly fragmented dolostones) were covered by debris. Therefore the majority of the structural data (i.e. attitude of joints, faults and kinematics of the fault surfaces) was collected within the volumes of fragmented dolostones. Most of the measured fault surfaces (Fig.4.4b) were characterized by a mirror-like finish.


Fig. 4.5: Outcrop 1. The reddish layers (here darker) belong to the Sciliar Fm. Original bedding is preserved even if the rock is heavily fragmented.

4.2.2 Outcrop 2: 500 m to the W of the village of Salobbi

Fault geometry, kinematics and preexisting structures

Outcrop (2) was located just to the north of the restraining fault bend, where the FFZ strikes ca. N-S. The fault zone was associated with a badland morphology also here, but the presence of a road cutting through the badland offered a ca. N-S oriented section of the fault zone for a length of ca. 120 m and a height of ca. 6 m. Measured faults and joints had quite dispersed attitudes (Fig.4.6) but a dominant set striking ENE-WSW was recognizable. The kinematics of the ENE-WSW striking
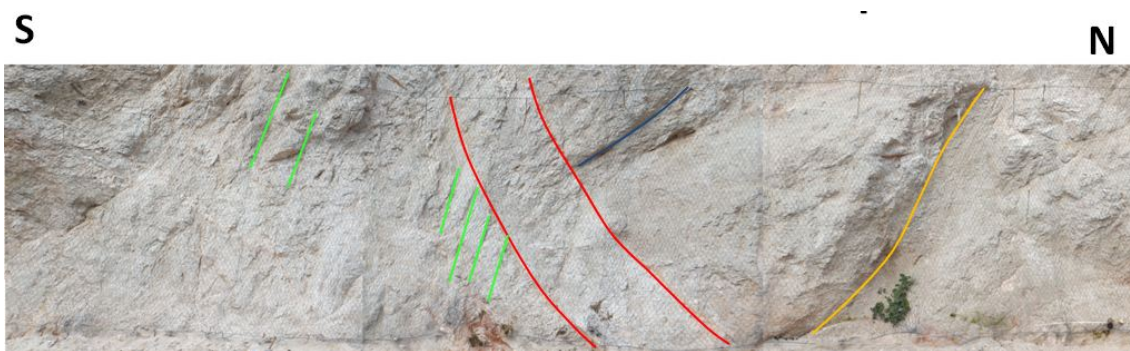
(a) The outcrop 2, N-S section
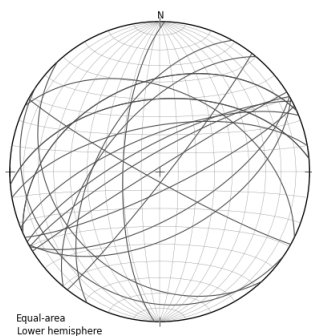
(b) Stereoplot of fault planes

(c) Example of dislocated greyish marker
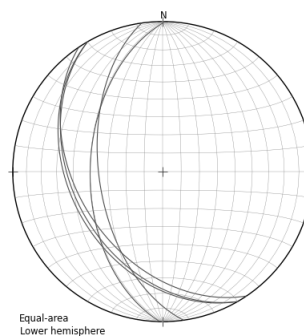
(d) Stereoplot of bedding

Fig. 4.6: Outcrop 2. (a) N-S oriented section of the FFZ along the road from Salobbi to Lauregno. The fault strands (black lines in the figure) have different attitudes. (b) Stereoplot of fault planes: a dominant ENE-WSW striking fault set is recognizable but the attitudes of the faults are quite scattered. (c) ENE-WSW striking fault cutting a dolostone marly horizon (parallel to the bedding) with 5 cm of reverse separation. (d) Stereoplot of the bedding at outcrop 2, to be compared with stereoplot (b). The dominant fault set cut through the bedding.

faults was dip-slip with reverse throws in the range 0.04-0.5 m determined thanks to the presence of offset structural markers such as bedding surfaces and horizons of marly dolostone. Basing on fault orientation and kinematics it seemed that the FFZ at outcrop (2) was still dominated by compressive structures such as within the restraining bend at outcrop (1). The bedding at outcrop (2) was dipping N240-270° with dip angles of 40-50°. Therefore, differently from outcrop (1), the dominant set of faults cut through the bedding (i.e., it does not exploit the bedding surfaces) (Fig.4.6).

Fault zone rocks

At outcrop (2) the FFZ was ca. 200 m thick and cut through two different facies of the Sciliar Fm.: a grey-in-color marly dolostone, and a white-in-color dolostone. Both the facies included intercalations of red clays, paleokarsts and paleosoils deposits. The fault zone was built by fragmented to highly fragmented dolostones (Tab.4.1) irrespective of the two different facies. Due to the orientation of the studied section (along the road), it was not simple to understand how the two classes of shattered dolostones were spatially arranged one respect to the other. Many of the fault surfaces were characterized by a mirror-like finish and by fault striae with few centimeters long hematite and goethite flames. The mirror-like fault surfaces typically cut through 2-3 mm thick gouge layers and sharply truncated the dolostone clasts within the gouge.

Fig. 4.7: Photograph of one of the best examples of mirror-like surface in the outcrop (2), with ca. 1 cm wide iron oxides-hydroxides flames.

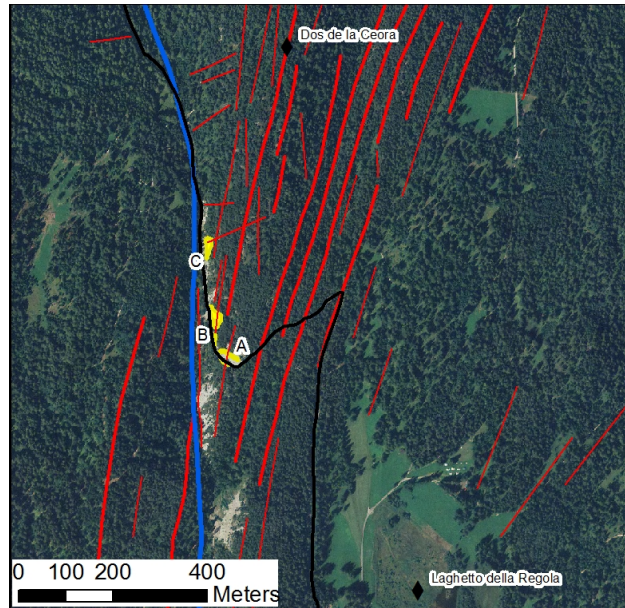### 4.2.3 Outccrop 3: locality of Doss de la Ceora

Fig. 4.8: Map of the Doss de la Ceora outcrops (yellow) along the Croce del Barba road (black in color), zoom of Fig.3.3. "A" refers to the outcrop oriented perpendicular to the fault; "B" and "C" are oriented about parallel to the FFZ trace (in blue). The thick red segments are the N 20° striking lineaments visible from remote sensing. The thin red lineaments are other minor faults-fractures recognized from remote sensing (see section 3).

Outcrop (3) was located along the road to Croce del Barba at the Doss de la Ceora ridge and consisted of three outcrops (A, B and C: yellow spots in Fig.4.8). Outcrop (A) was in an abandoned dolostone cobble quarry and exposed a ca. E-W oriented section of the FFZ; outcrop (B) was 50 m to the north from outcrop (A) along the same road and exposed a ca. N-S section of the fault zone; outcrop (C) was ca. 20 m to the north from outcrop (B) along the same road and had the same orientation of outcrop (B).

The main trace of the FFZ was not outcropping in the area, since it runs along a deep valley filled by alluvial deposits and located few meters to the west of outcrops (A), (B) and (C) (blue curve in Fig.4.8). The main fault was dipping N 270° with a dip angle of 80° (see Appiano geological map) and put in contact Permian volcanics of the GVA in the hangingwall block with Triassic dolostones of the Sciliar Fm. in the footwall block (see section 2.2.3. Therefore the studied outcrops offered variably oriented sections of the footwall block of the FFZ, which is cut by a stack of sub-parallel N 20-30° striking fault strands (4.8), well recognizable as lineaments

46

from remote sensing. These lineaments corresponded to trenches in the field. Here the FFZ is ca. 200 m thick. We performed several scan lines in the three outcrops which allowed us to describe the architecture of the FFZ perpendicular [outcrop (A)] and sub-parallel [outcrops (B), (C)] to fault zone strike. Along the scan lines, we distinguished five sets of faults and fractures (see table 4.2) and classified the damage of the fault rocks (see previous table 4.1). The bedding of the Sciliar Fm. was well recognizable, with strata 50-60 cm thick. Moreover the presence of stromatolite layers which mark the peritidal cycles allowed us to distinguish the bedding from joints (see Fig.4.2). Approaching the main trace of the FFZ the bedding was progressively rotated both in strike and dip angle up to be dragged along the fault (i.e., the average dip and dip-azimuth rotated from 20° -> N 205° to 80° -> N 290°: the latter attitude/strike is sub-parallel to the average fault strike from remote sensing analysis). Though the direction of movement of several faults was easily determined due to the presence of fault striae, the sense of shear was difficult to be established because (1) of the lack of structural markers (including slickenfibers) and (2) since most faults were strike-slip it was not possible to recognize any stratigraphic displacement. The application of the Riedel shear criteria to slipping zones at the microscale yielded ambiguous results (see section 5).
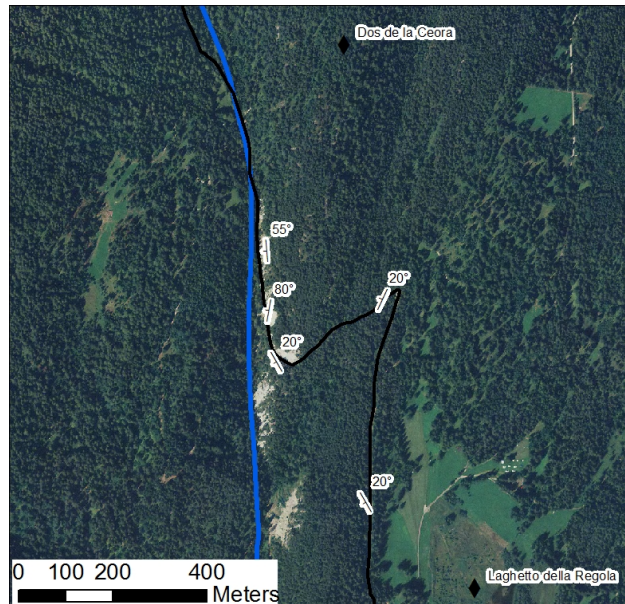

Fig. 4.9: Attitude of the average bedding in the Sciliar Fm. in the area of Dos de La Ceora, zoom of Fig.3.3. The rotation of the bedding surfaces approaching the main trace of the FFZ suggests dragging (and exploitation of these surfaces by the faults) of the strata during fault slip.

Scan lines orthogonal to the FFZ strike (outcrop A)

The structural data were collected along five scan-lines, four located to the north and one to the south of the road. The four scan-lines to the north of the road were striking N 99, 62, 93, 97° and were 5 m (scan 1), 10 m (scan 2), 8 m (scan 3) and 14 m (scan 4) long, respectively; the one to the south of the road (scan 5) was striking N 151 °, and was 20 m long. The dominant set of faults (red and orange great circles in the stereographic projection in Fig.4.10) was striking N 20-30° and steeply (> 75°) dipping mainly to the east This fault set was very persistent and locally had a regular spacing of 2-3 m (e.g. see scan line 4 in Fig.4.12b). These faults were parallel to the stack of lineaments recognized from remote sensing at the Doss de la Ceora and were often outcropping within small gullies. Because of this, the fault surfaces were rarely preserved. Other two secondary fault sets were recognized, one ca. E-W striking sub-vertical and another ca. WNW-ESE striking and dipping to the south with angles of ca. 60° which exploited the bedding (yellow and green great circles in Fig.4.10d respectively). At outcrop (A) the NNE-SSW striking main set of faults cut through the bedding. Some of the secondary faults displayed polished to mirror-like fault surfaces with fault striae consistent with dominant strike-slip kinematics (see Fig.4.18 for a summary of kinematic data of outcrop 3).

The fault zone consisted mostly of fragmented dolostones (F-type in table 4.1, orange diagonal lines in Fig.4.12) cut by tens of centimeters thick tabular lenses of highly fragmented dolostones (HF-type in table 4.1, blue diagonal lines in Fig.4.12). The bands of highly fragmented dolostones were often associated to the presence of the sub-parallel fault strands, and typically were cropping out within small erosive gullies. In some case the contact between fragmented and highly fragmented dolostones was marked by discrete, often mirror-like, fault surfaces. Therefore many of these faults were characterized by a strong asymmetry and in terms of off-fault rock damage intensity and of orientation of off-fault secondary fractures. On the other hand the fragmented dolostones were typically cut by four to five sets of joints and some secondary faults. The most persistent joint set was always that parallel to the NNE-SSW striking faults (see Fig.4.10a).

(a)   (b)

(c)   (d)

Fig. 4.10: Summary of the structural data from outcrop 3A. (a) Stereoplot of the poles of the joints (tot=73). (b) Stereoplot of the poles of the faults (tot=48). (c) Stereoplot of the bedding (great circles). (d) Stereoplot of the main fault families, striking: N 20° (red girdles); N 40° (orange girdles); N 70-80° (yellow girdles); N 110-120° (light green girdles). Only a selection of the main sets is presented here.
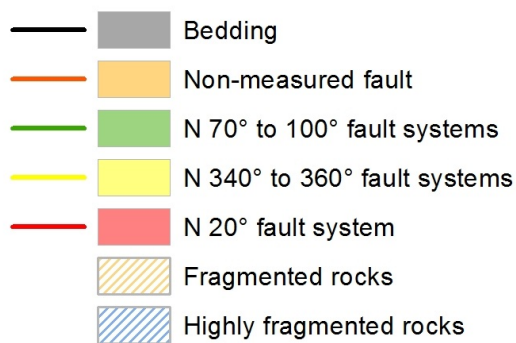
Fig. 4.11: Legend of Fig.4.12, 4.14 and 4.16
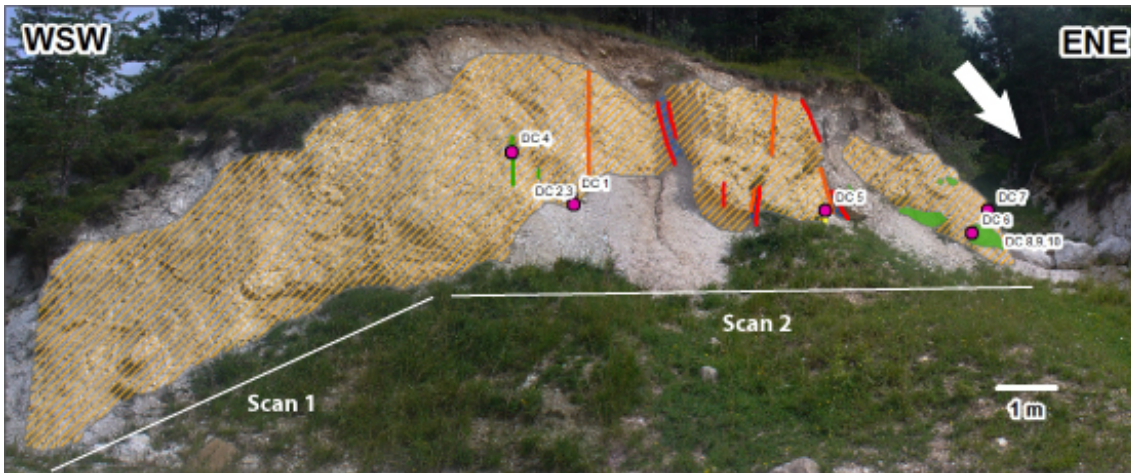
(a) Scan lines 1 and 2
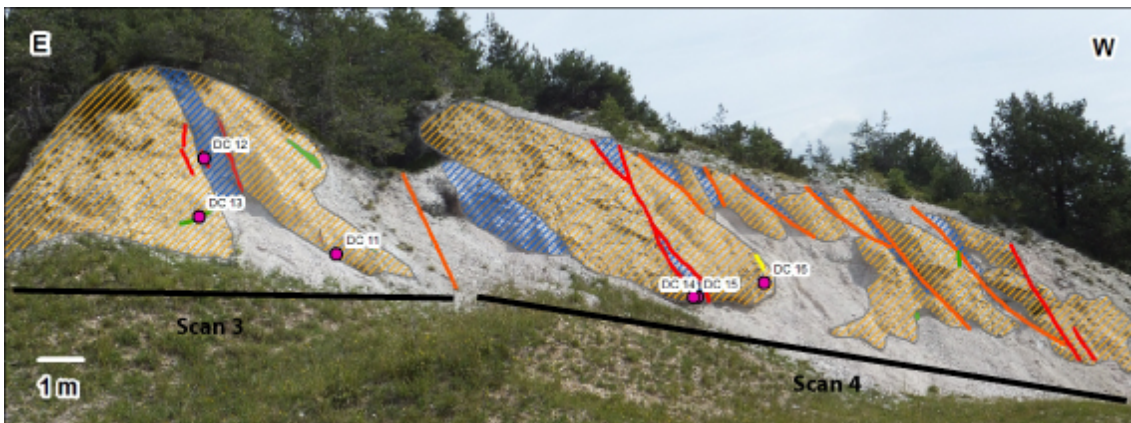
(b) Scan lines 3 and 4

Fig. 4.12: The first four scan lines allow to describe the damage zone and the fault traces in an orthogonal view to the FFZ average strike. Samples locations are indicated by red dots. Between the two sections the white arrow indicated the inferred trace of the fault core of one of the sub-parallel fault strands (these faults were clearly recognized from remote sensing survey: see Fig.3.4). For symbols, see Fig.4.11.

Scan lines parallel to the FFZ strike (outcrops B,C)

Outcrops (B) and (C) were very close to the trace of the main fault of the FFZ and were located just after outcrop (A) (Fig.4.8). They offered an almost continuous, 300 m long, exposure of the FFZ parallel to fault strike.

(a)   (b)
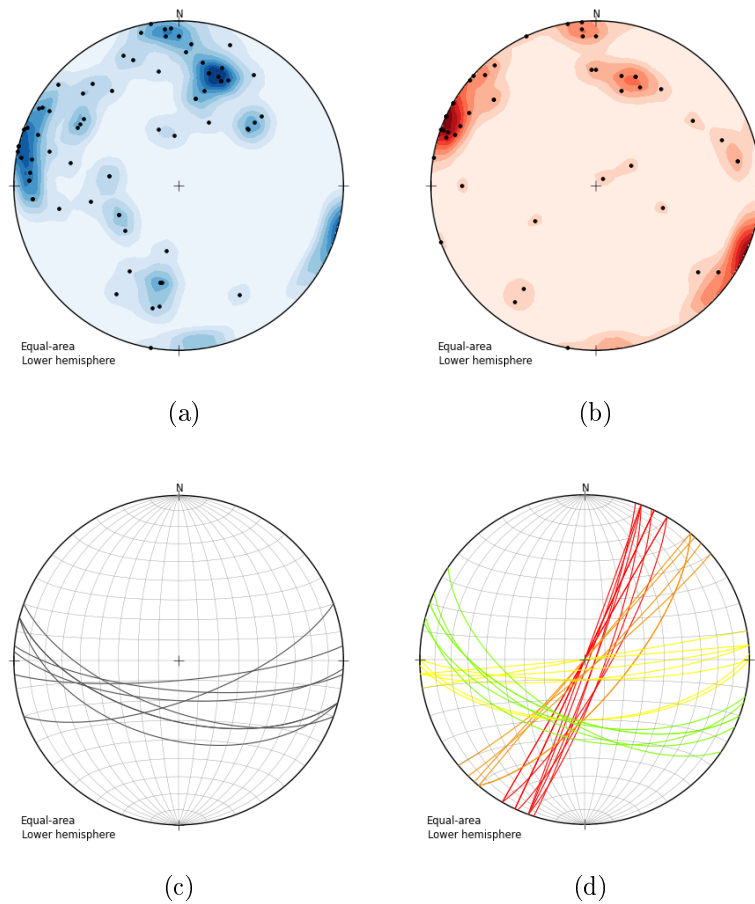
(c)   (d)

Fig. 4.13: Summary of the structural data from outcrop 3B. (a) Stereoplot of the poles of the joints (tot=45). (b) Stereoplot of the poles of the faults (tot=17). (c) Stereoplot of the bedding (great circles). (d) Stereoplot of the main fault families (great circles), striking: N 80-90° (yellow girdles), N 100-110° (green girdles), and N 10-20° ("Foiana type" trend, red-dashed girdles). Only a selection of the main sets is presented here.

Outcrop B   The outcrop consisted of large exposures of fractured dolostones and of a 3-4 m thick band of highly fragmented dolostones. The highly fragmented dolostones (HF-type in table 4.1) were concentrated along three sub-parallel fault strands belonging to the N 20° striking fault set (dashed-red great circles in Fig.4.13d). The fragmented dolostones were systematically cut by four to five sets of joints with the most pervasive one striking N 20°. Moreover a set of minor E-W striking faults was

Fig. 4.14: Outcrop B. Drag fold within the bedding (outlined with black lines). To the left, towards the road (and the creek, not shown) is indicated the kinematics of the main fault of the FFZ. The fault strands highlighted in red belong to the N 20° dominant fault set. Legend from Fig.4.11

also well recognizable (yellow and green great circles in Fig.4.13d).

The most interesting feature of outcrop (B) was the change of attitude of the bedding approaching the trace of the main fault of the FFZ. At outcrop (A) (ca. 50 m to the east of the main fault) the bedding dip azimuth was N200-220° and the dip angle ca. 60°. In the southern part of outcrop (B) (ca. 30 m to east of the main fault) the bedding dip azimuth was N 240-250° and the dip angle ca. 60°, whereas in the northern part of outcrop (B) (ca. 15 m to the east of the main fault) the bedding dip azimuth was N 260-280° and the dip angle 70-80°. Therefore it was evident that the bedding progressively rotated to become sub-parallel to the main fault trace of the FFZ. In the Fig.4.14 is clearly showed how bedding (black lines in the figure) was folded and dragged along the main fault (orange line with kinematics in the figure). In the folded area the bedding itself was frequently exploited by joints and new sets of joints striking N 110° developed.

Outcrop C This outcrop was characterized by three sub-parallel fault strands belonging to the N 20° striking fault set (dip azimuth N 290-300°, dip angle 80-90°) spaced 3-4 m apart. These three faults are hosted in a highly fragmented dolostones
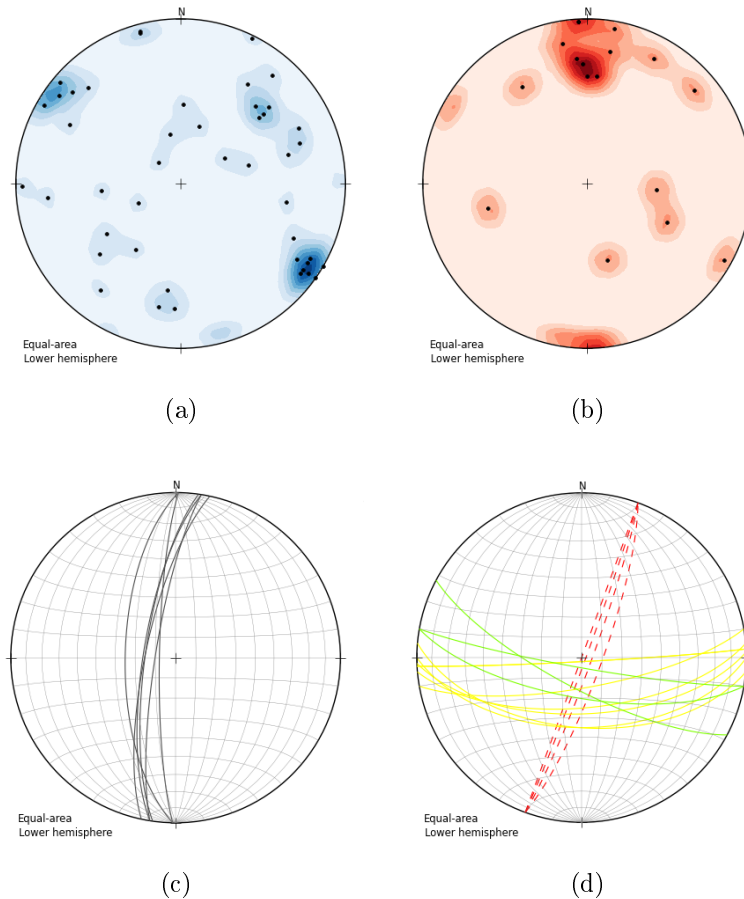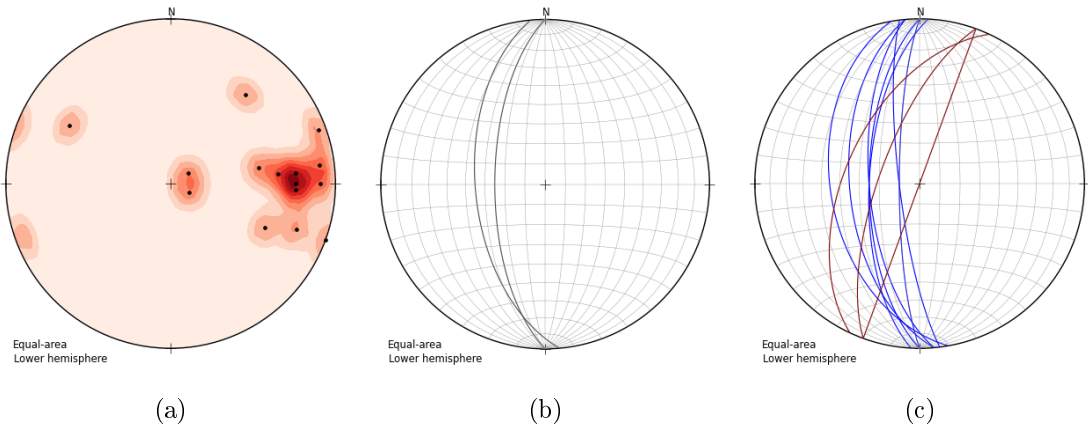
Fig. 4.15: Summary of the structural data from outcrop 3C. (a) Stereoplot of the poles of the faults (tot=17). (b) Stereoplot of the bedding (great circles). (c) Stereoplot of the main fault families (great circles), striking: N-S (blue girdles), N 20° (brown girdles). Only a selection of the main sets is presented here. The N-S faults have the same attitude as the bedding (compare (b) with (c)).

cut by a dominant joint set with spacing < 1 cm and parallel to the faults. One of the sub-parallel fault strands (red dashed line in Fig.4.13) puts in contact a white-in color dolostone with reddish-in color marly dolostone, both belonging to the Sciliar Fm. (Fig.4.17). Only along this fault it was recognizable a 6-8 cm thick layer of yellow to grey in color clay-rich gouge. Clays were made of kaolinite and smectite (XRD analysis performed by Michele Fondriest).

Another well-developed fault set had a dip azimuth N 260-275° and dip angle ca. 70° and exploited the bedding surfaces of the Sciliar Fm. (highlighted in yellow in the top right in Fig.4.16). This fault set displayed mirror-like slip surfaces with fault striae consistent with sinistral transpressive kinematics and was cut by the N 20° striking set. The N 20° fault set itself showed some fault surface with mirror-like finish.

Summary of the structural features of outcrop 3 (Doss de la Ceora)

Fault geometry, kinematics and preexisting structures   Outcrop 3 of the FFZ (locality of Doss de la Ceora) was characterized by the presence of a stack of sub-parallel fault strands striking N 20-30° (NNE-SSW) and spaced 4-50 m apart (see also section 3). Secondary fault sets were striking ca. E-W and ca. N-S, the latter reactivating the bedding. Fault kinematics had a dominant strike-slip

Fig. 4.16: Outcrop 3C. The three major N 20° striking faults (red segments). The fault colored with red-dashes segments puts in contact the white-in color dolostone with the reddish-in color marly dolostone, both belonging to the Sciliar Fm. (see Fig.4.17). The yellow polygon to the right represents the surface of a N-S striking fault exploiting the bedding of the Sciliar Fm. Traces of the bedding are outlined in black. Legend see Fig.4.11.

Fig. 4.17: Outcrop 3C. View looking to the north of the N 20° striking fault (brown line in Fig.4.15) which puts in contact the highly fragmented white dolostones to the east with reddish-in color fragmented marly dolostones to the west. All rocks belong to the Sciliar Fm.

to oblique-slip (i.e. pitch angles 20-40°) kinematics associated to a minor dip-slip, likely reverse, component measured in few faults (see Fig.4.18). The sense of shear was difficult to be established in the field, as discussed previously.

Fault zone rocks   Highly fragmented dolostones were less abundant with respect to outcrops 1 and 2, since they were concentrated only in up to 1-2 m thick bands around the sub-parallel fault strands. The FFZ at outcrop 3 was mainly built of fragmented dolostones. Mirror-like surface are not as widespread as in outcrop 2, because the majority of the faults cropped out within small erosive gullies. Nevertheless some faults, especially those belonging to the N 20° fault set or reactivating the bedding, displayed polished to mirror-like slip surfaces.
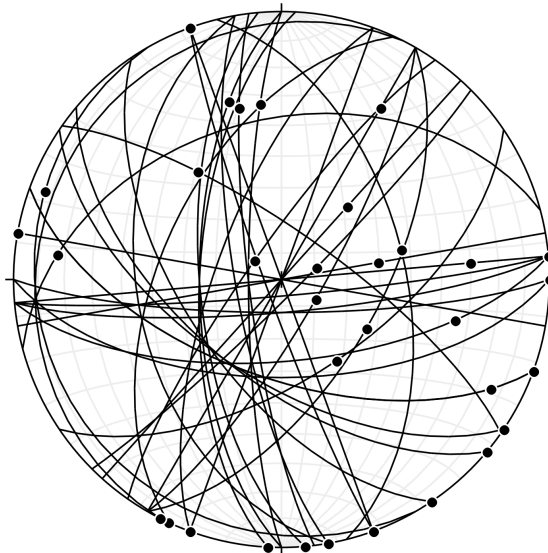

Fig. 4.18: Summary of the kinematic data of outcrop 3. Fault planes (great circles) with pitch (tot=37). See text for data description.

Joint set	Dip-azimuth	Dip
E-W	N 9-12°	33-90°
NW-SE	N 50-64°	33-35°
N-S	N 79-85°	45-78°
N-S	N 92-95°	80°
NNE-SSW	N 118-125°	70-90°
NE-SW	N 130-145°	60-85°
ENE-WSW	N 165-168°	25-84°
ESE-WNW	N 191-214°	35-80°
NW-SE	N 230-231°	45-50°
NNW-SSE	N 240-255°	25-68°
NNE-SSW	N 296-307°	65-90°
Fault plane set	**Dip-azimuth**	**Dip**
NNW-SSE	N 60-76°	35-90°
NNE-SSW	N 108-120°	78-90°
NE-SW	N 130-140°	70-90°
E-W	N 170-185°	60-90°
ESE-WNW	N 193-214°	50-85°
N-S	N 260-273°	45-80°
NNE-SSW	N 288-305°	35-80°

Tab. 4.2: Summary of the structural dataset of outcrop 3. Attitude consists in strike and dip angle

4.3   Summary of the field observations

The field observations along the FFZ can be summarized as follows.

- The FFZ consisted of intensely fragmented dolostones which seemed to be shattered *in situ* (i.e. no evidence of significant shear strain).

- The thickness of the FFZ decreased moving from the south (outcrop 1) to the north (outcrop 3) along fault strike. Moreover the proportion of highly fragmented (HF) dolostones with respect to the fragmented (F) one seemed to decrease moving from the south to the north.

- The scattering of the fault attitudes decreased significantly from the south to the north along the strike of the FFZ.

- The kinematics of the faults switched from dominant dip-slip reverse to dominant strike- to oblique-slip moving along the FFZ from the south to the north.

- Preexisting structures, such as the bedding, were frequently reactivated by

faults within the FFZ. In outcrop 3, the bedding was progressively dragged into the fault zone and the bedding surfaces exploited by the faults.

- Many fault surfaces cutting the shattered dolostones of the FFZ were characterized by extremely smooth fault surfaces with mirror-like finish (see section 5 for a description of the relative microstructures).

Chapter 5

Microstructures

In this section I refer to both the slip surfaces and the underlying slip zones when describing the samples. By definition, the slip surface corresponds to the fault surface itself, sometimes containing slickenlines and surface grooves that indicate the direction of slip. The slip zone, up to tens of centimeters thick, immediately underlies the slip surface and contains variably developed fault rock materials. Collectively, the slip surface and slip zone are thought to accommodate the bulk of fault displacement during the seismic cycle and mostly during individual earthquakes [Sibson, 2003, Smith et al., 2011]. To describe the rocks associated to the faults of the FFZ I tried to use the classification scheme of Sibson [Sibson, 1977]. But since many of the described rocks displayed different characteristics with respect to the "classical" cataclastic-type fault rocks, I also introduced a specific terminology.

The Foiana Fault Zone is characterized by large exposures (up to 300 m thick) of intensely damaged dolostones, which are pervasively fractured down to the micrometer scale (i.e. shattered dolostones). In the field, fractured dolostones are cut by discrete, centimeter-thick faults associated with extremely localized (down to few millimeters thick) slip zones. Many of the slip zones include ultra-polished mirror-like slip surfaces (they reflect the sun light). The shattered dolostones contain open (i.e., un-sealed) fractures and therefore the dolostones are very prone to be eroded. On the contrary, whitish and well-cemented cataclasites few centimeters thick are right below the slip surface.

The slip zones of both major and secondary faults were systematically sampled along the E-W oriented section of the Foiana Fault Zone at the Doss de la Ceora

(outcrop 3A, see section 4.1). Twenty-two oriented samples were collected to be representative of the different sets of faults recognized in the field. Since the majority of the faults cut through fragmented to highly fragmented dolostones (section 4.1, Fig.4.3 and Tab.4.1), some samples were preliminary consolidated with acrylic glue directly in the outcrops. Among these, twelve samples were consolidated with epoxy resin at Dept. of Geosciences in Padua and cut to produce polished thin sections oriented perpendicular to the fault surfaces and parallel to fault lineations (see Tab.5.1).

Microstructural investigation of the slip zones was performed using a Nikon LABOPHOT-2 optical microscope and a Camscan MX 2500 Scanning Electron Microscope (SEM) at the Dept. of Geosciences in Padua. Moreover, few thin sections were also observed under optical microscopy cathodoluminescence (OM-CL) to unravel the role of fluids and veining during faulting. Most of the microstructural investigation was conducted at the optical microscope by taking photomicrographs or analyzing high-resolution (5-10 μm of spatial resolution) optical scans of the thin sections (the scans were performed by Stefano Castelli).

The two main goals of the microstructural investigation were: (i) characterization of microstructural features to understand the deformation processes in the slip zones during faulting, and (ii) recognition of kinematic indicators at the microscale to determine the sense of shear of the fault sets recognized in the field.

However, the arrangement of microfractures didn't allow in most of the cases the unambiguous definition of the shear sense, because the prevailing fractures were randomly-oriented, with few displacement and lateral continuity. An exception to this difficulties can be seen in Fig.5.6a.

Sample - DC	Dip direction	Dip angle	Pitch	Orientation	Fault set
1N	175	90	0	N block	E-W
1S	175	90	0	S block	E-W
2	120	90	27	-	N 20°
4	10	90	-	S block	N 100°
6	200	60	15	Fw block	N 110°
8	135	85	60	-	N 45°
9	135	85	85	NW block	N 45°
10	180	60	0	Fw block	E-W
11A	35	75	50	-	N 125°
11B	170	90	60	-	E-W
14	115	90	-	E block	N 25°
18	214	60	0	S block	N 124°

Tab. 5.1: Samples selected for the microstructural study. Sample location is shown in Fig.4.12.

5.1 Microstructural features within the slip zones

"Classical" slip zones cutting both carbonate- and silicate-bearing rocks described in literature consist of few millimeters to tens of centimeters thick cataclasites passing to very localized ultracataclastic layers in proximity of the slip surfaces [Chester and Chester, 1998, Wibberley et al., 2008, Smith et al., 2011]. Cataclasites are cohesive fault rocks characterized by the presence of subangular to rounded clasts immersed in a matrix of fine grain material mainly derived from clast abrasion or precipitated from pore fluids. Cataclasites are the result of comminution and frictional sliding. Following Sibson [Sibson, 1977] fault rock classification (see Fig.5.1), cataclasites are distinguished on the base of clasts vs. matrix volume ratio in protocataclasites (10-50% matrix), cataclasites (50-90% matrix) and ultracataclasites (>90% in matrix) . When the matrix content is less than 10% in volume, the fault rocks are called breccias. Depending on the size of the fragments, breccias are distinguished in crush breccia (fragment size > 0.5 cm), fine-crush breccia (fragment size 0.1 - 0.5 cm) and crush microbreccia (fragment size < 0.1 cm). Both cataclasites and breccias accommodate shear strain.

In our case study, most of the sampled faults cutting shattered dolostones were characterized by polished to mirror-like slip surfaces with up to 5 mm wide fault striae often lined by brownish flames of smeared oxides and hydroxides. Such slip surfaces showed very smooth profiles in thin section (i.e. surface undulations of few

Cohesive						Incohesive		
	Nature of matrx					Fault gouge (visible fragments <30% of rock mass)	Fault breccia (visible fragments >30% of rock mass)	Random fabric
Grain growth pronounced	Tectonic reduction in grain size dominates grain growth by recrystallization and neomineralization				Glass/devitrified glass			
	Cataclasite series			Crush breccia (fragments >0.5 cm) / Fine crush breccia (0.1<fragments<0.5 cm) / Crush microbreccia (fragments <0.1 cm)	Pseudotachylyte			
Blastomylonite	Ultracataclasite	Cataclasite	Protocataclasite			Foliated gouge		Foliated
	Mylonite series							
	Ultramylonite	Mylonite	Protomylonite					
	Phyllonite series							
	90–100	50–90	10–50	0–10				
	Percent of matrix							

Fig. 5.1: The fault rocks classification from [Sibson, 1977].

micrometers at length scale of about 1 mm) (see Fig.5.4) and sharply cut the slip zone material below. A typical feature related to the extreme shear strain localization along the slip surfaces was the presence of truncated clasts (Fig.5.4c).

The fault rock fabric below the slip surfaces was significantly different from that expected for rocks dominated by cataclastic processes (e.g. sub-angular to rounded clasts, presence of matrix, evidence of shear fracturing). In particular, the most striking characteristic of the FFZ slip zones was the absence of significant shear strain even at distances of few tens to hundreds of micrometers from the slip surfaces (see Fig.5.2). These features do not correspond to microbreccias nor to ultracataclasites.

A series of microstructural features indicate that the fabric of the slip zones was dominated by *in situ* shattering processes (see Fig.5.5, 5.3 and 5.2). Such microstructural features consisted of:

- Exploded clasts affected by radial fractures. Each clast fragment had its counterpart and no significant shearing was recognizable (Fig.5.5e and 5.5f).

- Pervasive and variably oriented extensional fracturing and splitting of clasts down to the micrometer scale (Fig.5.5a).
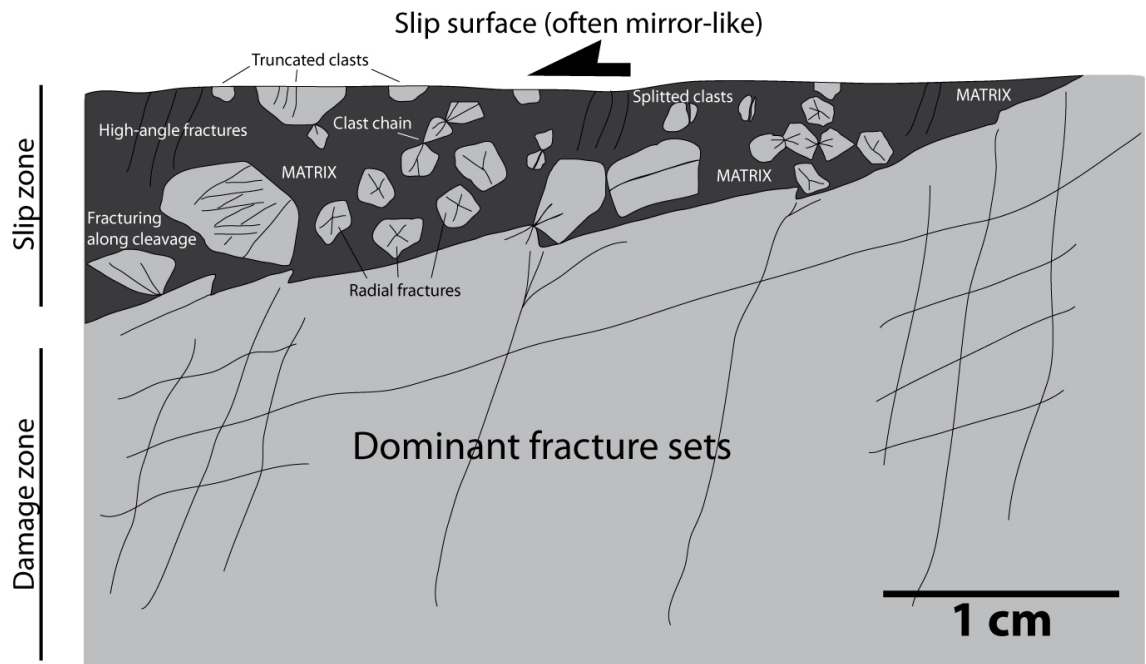
62

Fig. 5.2: A very conceptual scheme indicating the slip zone peculiar characteristics. The slip zone is wedge-shaped because this feature is observed and also in order to represent the variability of its thickness in our thin sections, from 0 to 40 millimeters at least (i.e. the whole thin section). Radially fractured, indented, splitted, truncated and disposed in chains clasts are represented. The sets of fractures oriented up to 80° to the slip surface are also drawn.

- Presence of chains of splitted clasts (resulting from force chains) oriented at 60-80°to the slip surfaces (Fig.5.5b and 5.5c).

Thanks to the usage of OM-CL techniques it was possible to confirm the lack of shear strain. An example is presented in Fig.5.3, where the same triangular shaped algae fragment is observed by OM-CL and OM plane-polarised nicols (OM-PPL). Thanks to the cathodo image, it's possible to see a dark rim all around the fragment, which appears in optical continuity. In the other image, instead, the fragment appears cut by many fractures. Combining the two observations, those fractures cutting through the algae clast are lacking of shear strain.

In general, the fracture pattern affecting these shattered fault rocks had no evident preferential orientation. Nevertheless, in some cases and only within a damage zone few millimeters thick bordering the slip surface, a fracture set at high angle to the slip surface (60-70°) with regular spacing was recognized (see Fig.5.6).

Microstructural features similar to those described here (i.e., pervasive fragmentation and absence of evidence of shearing) are typical of pulverized rocks, though
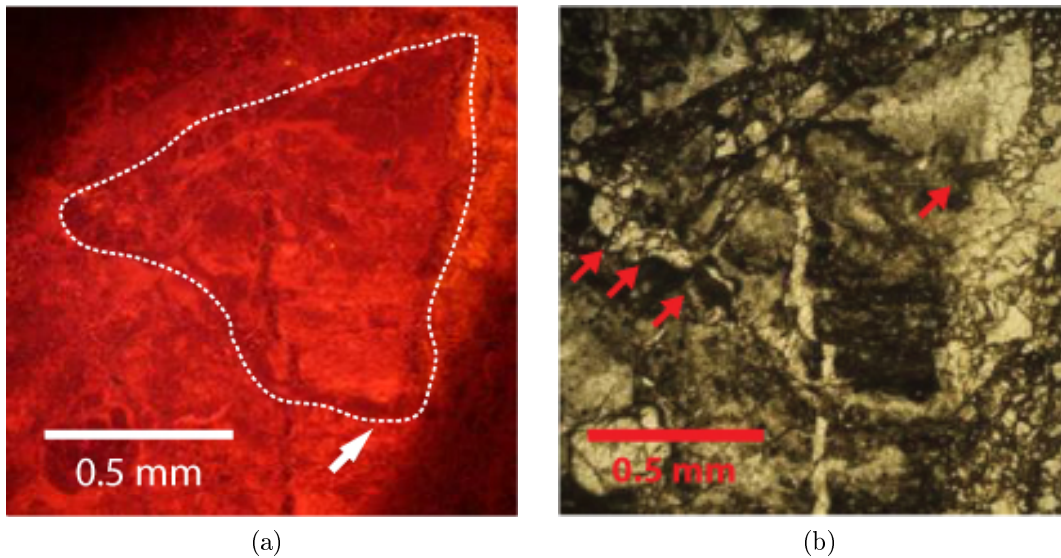
63

(a)	(b)

Fig. 5.3: Triangular shaped algae fragment (dolomitic in composition). The comparison of OM-CL (a) with OM-PPL (b) images of the same fragment. A dark rim, evidenced from a white arrow in (a), indicates the optical continuity of the fragment, even if is cut from fractures, as indicated by red arrows in (b).

in that case the size of the fragments is often below 1 m, while here the fragment size is ca. 1 mm [Dor et al., 2006, Dor et al., 2009]. Pulverized rocks are interpreted as the product of intense stress perturbation in the rock volume near the rupture tip induced by the propagation of the rupture tip and near source elastic wave propagation [Reches and Dewers, 2005, Dor et al., 2006, Dor et al., 2009, Ben-Zion and Shi, 2005]. Pulverized rocks are typically found near the surface (< 2 km in depth), where the confining pressures are small allowing intense extensional fracturing [Dor et al., 2006, Dor et al., 2009]. The possible mechanisms of formation of the shattered dolostones of the FFZ will be discussed in section 6.
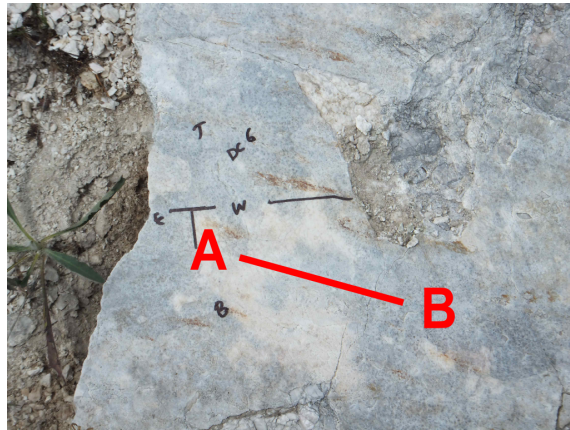
(a)
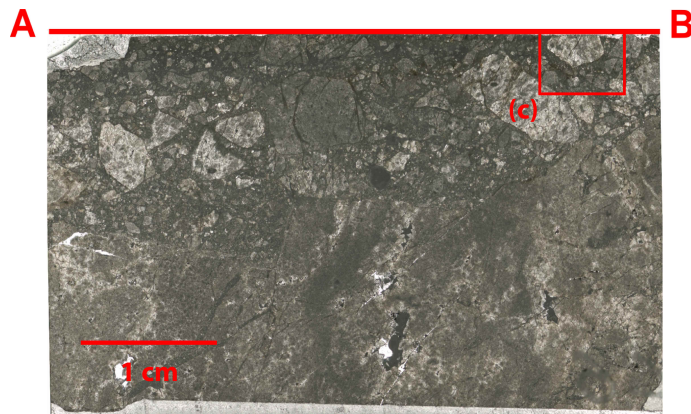
(b)
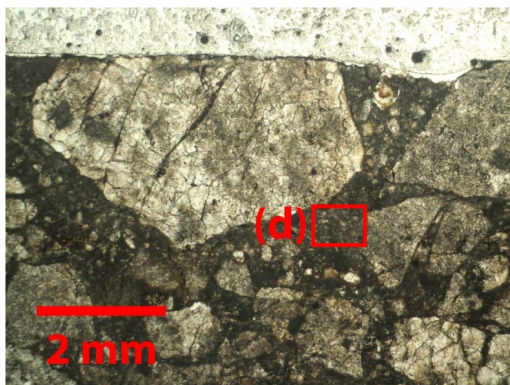
(c)
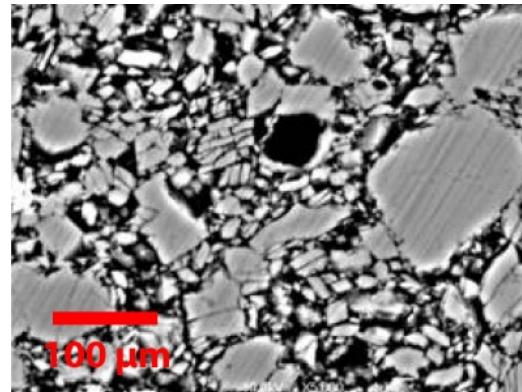
(d)

Fig. 5.4: Field structures and microstructures of the fault surfaces and slipping zones (examples from Doss de la Ceora, sample DC 6). (a) Field image of a mirror-like slip surface with lineations made by reddish in color iron-rich oxides/hydroxides . The slip surface truncates dolostone grains. (b) Scan of the thin section (45 mm in length) cut perpendicular to the fault surface and parallel to the lineation along A-B in (a). The transition from the slip zone to the almost un-deformed rock beneath is very sharp. (c) Truncated clast (box in Fig.5.4b) close to the slip surface: the presence of a polished truncated grain suggests high shear strain localization (OM-PPL image). (d) Matrix within 1 mm from the slip surface. Extensional fracturing, often exploiting dolomite cleavage, produces fragments smaller than 250 nm (SEM-BSE image).

(a)   (b)

(c)   (d)

(e)   (f)
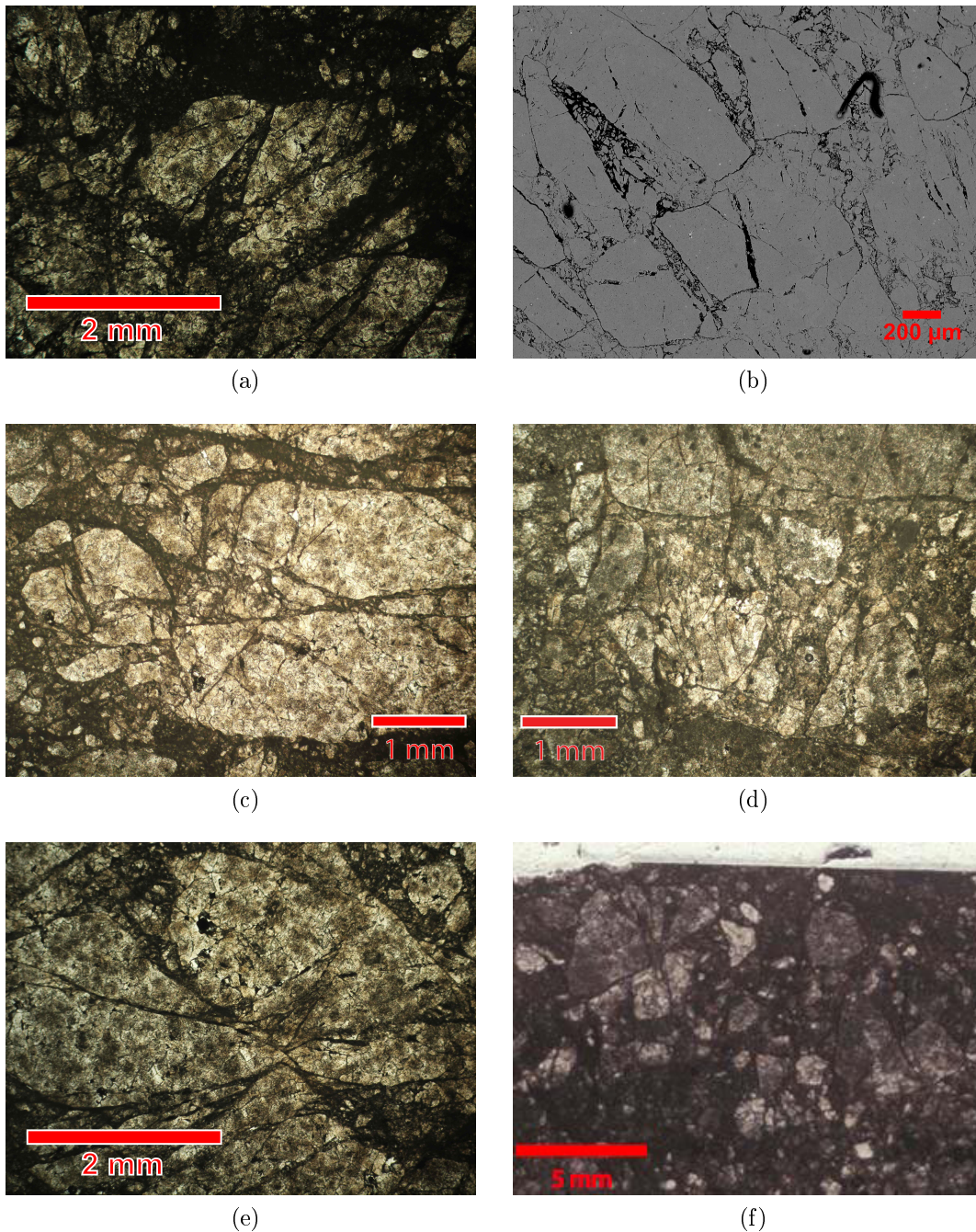
Fig. 5.5: Microstructures of the fragmented clasts bordering the slipping zones (examples from Dos de la Ceora). All the images are oriented with the slip surface located to the top and parallel to the long side of the image. (a) and (b) Split clasts located at 5 mm from the slip surface with the tensional fractures oriented at high angle with respect to the slip surface (OM-PPL and SEM-BSE images, respectively, from sample DC 1S). (c) and (d) Indented clasts located within 2 mm from the slip surface (OM-PPL images, from samples DC 2 and DC 6). (e) and (f) Radial fracturing of clasts located within 2 mm from the slip surface (OM-PPL and SEM-BSE images, respectively, from sample DC 1S and one in outcrop 2). These microstructures suggest impacts and *in-situ* shattering of the rock next to the slipping zones.
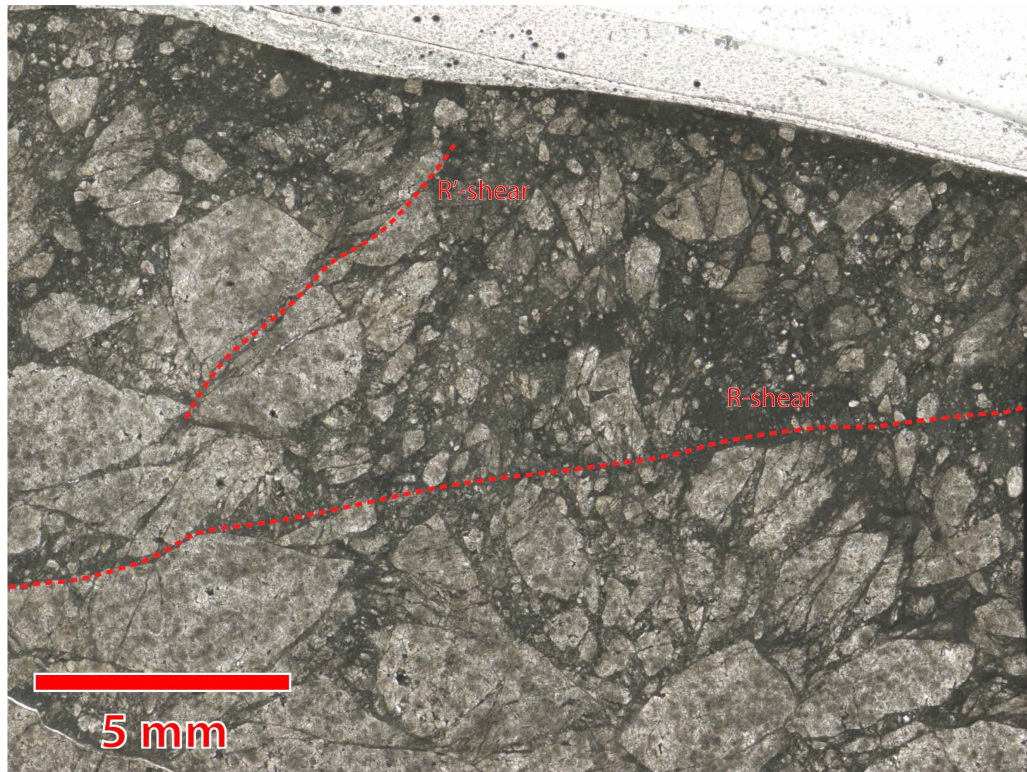
(a)
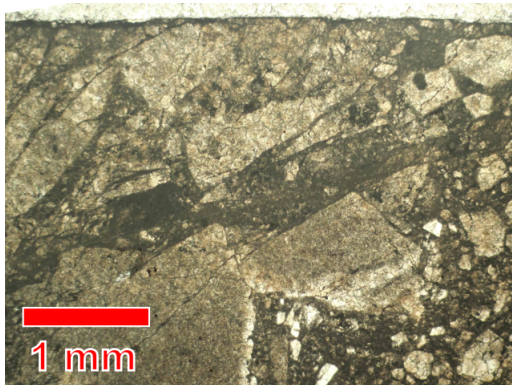
(b)
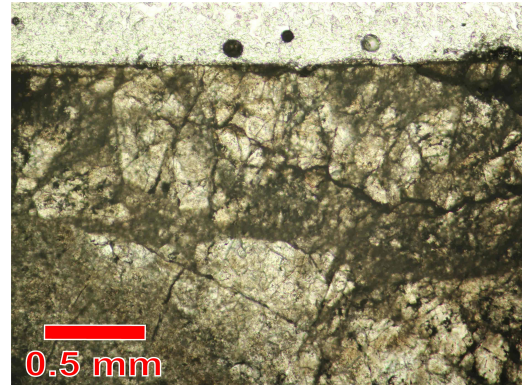
(c)

Fig. 5.6: Pervasive clast splitting in the slip zone. All thin section were cut perpendicular to the fault surface (located to the top) and parallel to the slip direction, the angles reported are referred to the slip surface. (a) Slipping zone with prominent 20° angle fracture all across the image, interpreted as R-shear and radial fracturing with clast splitting immediately below. Also a set of smaller fractures, inclined of about 60°, are present close to the slip surface, to the center, while only the red-dashed shows displacement and is interpreted as R'-shear (optical scan, sample DC 6). (b) Low-angle opening mode fracture (OM-PPL image, sample DC 8). (c) High-angle fracture set (OM-PPL image, sample DC 11B).

Chapter 6

Discussion

The aim of this thesis is the determination of the architecture of an exhumed ancient seismogenic fault in dolostones as an example of active seismogenic sources hosted in carbonates. Since there are no clear "structural" indicators of ancient seismic ruptures in carbonate-built rocks (see section 1), in this section I first discuss the seismic origin of the microstructures found in the fault rocks of the FFZ (section 6.1) and then the architecture of the FFZ (section 6.2). Lastly, I discuss the relationships between the architecture of the FFZ and individual seismic ruptures (section 6.3.1 and 6.3.2) and compare the architecture of the FFZ with the architecture of an active strike-slip fault inferred from seismic waves inversion analysis (section 6.3.3).

6.1 Evidence of ancient seismic ruptures within the FFZ

Field and microstructural observations carried out in this thesis highlighted the occurrence of peculiar structural features within the FFZ, which namely were: (i) in-situ shattered (fragmented to highly fragmented or "pulverized") dolostones (section 6.1.1), (ii) faults with mirror-like slip surfaces (section 6.1.2), (iii) slipping zones with radially-fragmented clasts, and (iv) clasts truncated by mirror-like surfaces. Here below I discuss how these four structural features can be interpreted as the result of ancient earthquake ruptures propagating along the FFZ.

6.1.1 *In situ* shattered ("pulverized") dolostones

In-situ shattered dolostone rocks are a common feature of the FFZ. An intense degree of fracturing results in rock pulverization. Pulverized fault rocks were firstly reported by Brune [Brune, 2001] along the San Andreas Fault at Tejon Pass. These rocks were unique in comparison to other fault rocks since they (i) appeared to have been shattered in-situ, (ii) had very fine grain size (i.e. < 1 mm) due to intense fracturing, and (iii) did not display evidence of significant shear strain. Actually such pulverized rocks preserved all primary features of the local host rocks, which were granites and gneisses, but were easily reduced into powder by hands when taken out from the outcrops. To date, pulverized rocks have been reported along some major (i.e., hundreds to thousands kilometers long) strike-slip faults, such as several faults strands of the San Andreas system in California [Brune, 2001, Wilson et al., 2005, Dor et al., 2006, Dor et al., 2009, Rockwell et al., 2010, Rempe et al., 2013], the North Anatolian Fault in Turkey [Dor et al., 2008] and the Arima-Tatatsuki Tectonic Line in Japan [Mitchell et al., 2011]. In all these cases pulverized rocks developed mainly within crystalline host rocks (i.e., igneous or metamorphic) with the exception of a sandstone outcrop along the San Andreas Fault [Dor et al., 2009]. Moreover, to my knowledge, the only example of pulverized rocks within carbonate host rocks was reported by [Agosta and Aydin, 2006] along the Venere Fault (Central Apennines, Italy). Such fault rocks consisted of a 1 m thick band of finely comminuted (maximum rock fragment size ca. 1 cm) limestones with preserved sedimentary layering and parallel to the fault core. The intensely fractured rocks (shattered dolostones) of the FFZ and the fractured rocks of Venere Fault are larger in average grain size than the so-called pulverized rocks found in the silicate-built rocks. Nevertheless the true origin of these rock (i.e., in-situ shattered limestones and dolostones and pulverized silicate-built rocks) has still to be conclusively established.

Several authors suggested that pulverized fault zone rocks are of coseismic origin based on both theoretical and experimental argumentations. Brune [Brune, 2001] suggested that sliding on a rough fault during earthquakes at seismogenic depth might generate intense variations in normal stress able to fracture the wall rocks of the fault. According to this model successive earthquake ruptures might cause repeatedly fracturing of the rock mass to very fine grain sizes without clear appar-

ent shear. Ben-Zion and Shi [Ben-Zion and Shi, 2005] simulated extensive off-fault plastic yielding by propagating dynamic ruptures along faults separating media with different elastic properties (i.e. bi-material interfaces). The ruptures propagating along such interfaces are named "wrinkle-like pulses" and are typically associated to the generation of a strong extensional loading within the medium characterized by the higher shear wave velocity (i.e., the stiffer medium). Repeating occurrences of ruptures propagating from depth and with the same directivity is expected to produce strongly asymmetric rock damage and possibly pulverization around these faults. This expectation is consistent with the asymmetric distribution characterizing many pulverized rocks with respect to bi-material faults (e.g., some segments of the San Andreas Fault). From the experimental point of view, Doan and Gary [Doan and Gary, 2009] and Yuan et al. [Yuan et al., 2011] used Split Hopkinson Pressure Bar tests to investigate high strain rate deformation in granites. They demonstrated that granite pulverization occurred at very high strain rates (ca. 150 s^{-1}) and very small accommodated strains. Similar experiments performed on Carrara marble suggested that marble was easier to be "pulverized" compared to granite [Doan and Billi, 2011]. Such extremely high strain rates leading to rock pulverization are consistent with the strong stress perturbations transiently produced within the host rocks by the passage of earthquake ruptures along a fault. Anyway rock pulverization is expected to occur only up to a maximum depth of 3-4 km, where confining pressures are low and can be dynamically exceeded by off-fault stress perturbations induced by rupture propagation and the intense radiated seismic field. This is confirmed by both field studies on natural pulverized rocks and experimental observations [Yuan et al., 2011].

Fragmented and highly fragmented dolostones which characterized the FFZ displayed characteristics typical of pulverized rocks at the meso-scale, such as: (i) *in situ* shattering and absence of significant shear strain, (ii) preservation of primary sedimentary structures, and (iii) pervasive extensional fracturing down to millimeter scale in the field. At the micro-scale the presence of (i) exploded clasts with radial fractures, (ii) pervasive and variably oriented extensional fracturing and splitting of clasts down to the micrometer scale, and (iii) clast impingement, is also consistent with microstructural observations reported for both natural and experimentally-

produced pulverized rocks [Dor et al., 2009,Doan and Billi, 2011,Rempe et al., 2013].
Based on these observations I interpret the fragmented and highly fragmented (in-
situ shattered) dolostones within the FFZ as "pulverized dolostones", which would
represent the product of coseismic damage due to the propagation of earthquake
ruptures along the FFZ.

The asymmetric distribution of pulverized rocks across faults was frequently
described in literature and was used to infer preferential directivity of ancient earth-
quake ruptures [Dor et al., 2006,Mitchell et al., 2011]. In the case of the FFZ, the
exposed sections were hosted in extensively "pulverized" dolostones. The peculiar
exposure is probably due to the strong lithological control on fault damage. Even
though the presence of pulverized rocks in other lithologies of the FFZ cannot be
excluded due to the lack of outcrops, the absence of badlands makes the occurrence
of pulverized rocks in these locations unlikely. In the southern sector of the FFZ
(outcrops 1, 2 in Fig.4.1), in correspondence to the restraining fault bend, it was not
possible to clearly define the distribution of the "pulverized" dolostones with respect
to the trace of the main fault of the FFZ. In the case of the Doss de la Ceora outcrop
(outcrop 3) it was observed a quite clear asymmetric distribution of the pulverized
dolostones, which were located in the footwall block (i.e. to the east in the map
view) with respect to the trace of the main fault of the FFZ (see Fig.4.8). A similar
damage asymmetry was also observed across some of the N 20° fault strands mapped
in the field. These very preliminary observations need to be reinforced by further
investigations (e.g., systematic studies of microfracture orientation in the slip zones
of the individual faults) to do some inferences about rupture directivity along the
FFZ.

6.1.2   Faults with mirror-like slip surfaces

The other striking feature within the FFZ is represented by the faults with mirror-
like slip surfaces cutting through the pulverized dolostones. These faults were easily
recognized in the field because they reflect the sunlight. According to the Rayleigh
roughness criterion a surface can reflect natural sunlight (wavelength 550 nm) if
the amplitude of the surface roughness is < 100 nm at a length scale L $=$ 550
nm [Siman-Tov et al., 2013]. This implies that mirror-like slip surfaces of the FFZ

were extremely smooth at the microscale. Mirror-like slip surfaces were widespread within the FFZ, especially in its southern sector (outcrops 1, 2), where they consisted mostly of small displacement (0.02 - 3.5 m) reverse faults.

A dedicated experimental study has been performed by Fondriest et al. (in press) to understand the origin of these mirror-like slip surfaces. Slow- to high-velocity experiments were performed on dolostone gouges using a rotary shear apparatus (SHIVA, INGV, Rome) at deformation conditions approaching those estimated for the Foiana Line: normal stresses up to 26 MPa, displacements in the range 0.02 - 3.5 m and slip velocities ranging from sub-seismic to seismic in the interval 0.0001 - 1.13 ms^{-1}. Mechanical data coupled with surface roughness measurements (using White Light interferometry) and microstructural observations of the experimentally-deformed gouges indicate that mirror-like slip surfaces (obeying the Rayleigh roughness criterion) (i) were formed only for seismic slip velocities (> 0.1 ms^{-1}) at the applied normal stresses, (ii) were related to dynamic weakening (i.e. drop of both shear stress and friction coefficient), (iii) were associated to extreme strain localization within the gouge (all shear strain was accommodated within up to 20 μm thick slip zones). At these deformation conditions the frictional power density (shear stress $\times$ slip velocity) dissipated in the gouge was comparable to that estimated for natural earthquakes (1-10 MWm^{-2}). These results indicate that small-displacement mirror-like slip surfaces in dolostone gouges were produced by extreme frictional power dissipation during seismic slip and therefore represent markers of seismic faulting. Mirror-like slip surfaces were previously observed to form during experiments at earthquake-like slip velocities also within other carbonate gouges such as calcite and siderite [Han et al., 2007, Smith et al., 2013] and extensively described in the field within fault zones cutting limestones [Siman-Tov et al., 2013].

Mirror-like slip surfaces within the FFZ had surface roughness and microstructural characteristics well comparable to the experimental ones (Fondriest et al., in press). The microstructural study performed in this thesis on the slip zones of the faults at the Doss de la Ceora (outcrop 3) further highlighted the extreme shear strain localization characterizing dolostone gouges in proximity to the mirror-like slip surfaces. The most significant evidence of such localization was the sharp truncation of the dolostones clasts along the polished and mirror-like slip surfaces.

6.2 Complexity of the FFZ architecture

The main topic of this thesis was the characterization of the FFZ architecture at different scales moving along fault strike from the southern sector of the fault (near the fault tip and the restraining bend) towards the north. At the scale of the remote sensing structural analysis (Section 3), the architecture of the FFZ was described on the basis of the scattering of the strike of the lineaments with respect to the mean strike of the fault zone. The main observation was that in the southern sector of the FFZ the lineaments were scattered around a dominant strike of N 40-50°, consistent with the strike of the FFZ restraining bend, while moving to the north at the Doss de la Ceora the lineaments were more clustered around a mean strike of N 20° with well-developed sub-parallel fault strands (Fig.3.4). At the scale of the field work (Section 4) moving from the south to the north along the FFZ strike (i) the average fault zone thickness decreased from 300 m to 200 m, (ii) the fault rock damage was more localized (the proportion of highly fragmented dolostones with respect to fragmented ones was significantly reduced), (iii) the scattering of fault attitudes decreased, and (iv) the kinematics of the faults switched from dominant dip-slip reverse to dominant oblique- to strike-slip. All these observations indicate that the FFZ became wider and more "complex" approaching the southern fault tip. The thickening of the fault zone and the concentration of the off-fault damage in correspondence to the fault tips is a frequently reported field observation about fault zones and is also predicted by several models of fault zone growth [Mitchell and Faulkner, 2009]. Moreover in the case of the FFZ the geometry of the fault at the regional scale had a further strong influence on the fault zone structure and kinematics. Indeed, with respect to a principal compressive axis striking N 340° (Valsugana deformation phase, section 2) active during faulting, the southern sector of the FFZ (striking N 40-50°) consisted of a restraining bend dominated by dip-slip reverse fault kinematics. Instead, towards the north, at the Doss de la Ceora (average strike N 20°) the FFZ was dominated by oblique- to strike-slip kinematics.

Another factor of complexity within the FFZ was represented by the bedding surfaces of the dolostones which were frequently exploited by the faults. This is a common situation in carbonate sedimentary sequences, where fault zone structure is strongly controlled by preexisting anisotropies such as bedding surfaces, veins,

pressure solution seams and joints [Graham et al., 2003, Agosta and Aydin, 2006, Hausegger et al., 2010]. Within the southern sector the individual faults, often with mirror-like slip surfaces, exploited the overturned bedding surfaces at the eastern limb of a fault propagation anticline across all the fault zone thickness (ca. 300 m, Fig.4.5). Instead, towards the north, at the Doss de la Ceora, the bedding was dragged and reactivated by the individual faults, often with mirror-like surfaces, but only at distances of few meters at most within the main trace of the FFZ (Fig.4.14).

6.3   Seismic ruptures and structural complexity

As previously discussed, the association of pulverized dolostones and faults with mirror-like slip surfaces is interpreted to record the propagation of ancient seismic ruptures along the FFZ. Based on this conclusion here I discuss the structure of the FFZ (i.e., an exhumed seismogenic fault in dolostones) (i) relative to the effects of individual seismic ruptures in the footwall rocks , (ii) in comparison to the results of earthquake rupture simulations along strike-slip faults, and (iii) in comparison to the structure of active seismogenic sources hosted in carbonate rocks.

6.3.1   Cumulative effects of individual seismic ruptures in the footwall rocks

A speculative interpretation about the distribution of the damage zone along the FFZ could be the following. The southern part of FFZ, including the fault restraining bend, is close to the main fault tip. The development of the 300 m thick pulverized rock belt in the footwall can then be explained by the cumulative number of individual seismic ruptures stopping at the southern fault tip. In general, the propagation of an earthquake rupture induces an intense stress field perturbation at the rupture tip and in the neighbor wall rocks (the latter due to the passage of the seismic wave front). Depending on the rupture directivity (= direction of propagation of the rupture) and on the sense of shear, the stress perturbation in the wall rocks could be tensional or compressional: this could result in a damage asymmetry in the wall rocks bordering the fault [Di Toro et al., 2005]. In the case of the FFZ, given the sinistral sense of shear, seismic ruptures propagating towards the south would result

in extensive damage in the footwall (i.e., the tensional quadrant would be to the SE). Actually, the largest outcrop (badlands) of "pulverized" dolostones is located in the eastern wall rock of the southern tip of the FFZ, so in correspondence of the SE (tensional) quadrant for seismic ruptures propagating from north to south in a sinistral fault (see Fig.6.1). Close to the southern termination, the FFZ bends and behaves like a reverse fault, fading into the km-scale anticline structure which transfers the deformation from the FFZ to the Trento-Cles Line (Fig.4.1). Fault bends (together with structures as dilational/contractional jogs and restraining bends) are thought as structures which arrest rupture propagation [King and Nábělek, 1985], thus fulfilling the previous discussion about the variations in "pulverized" dolostone thickness along-strike.
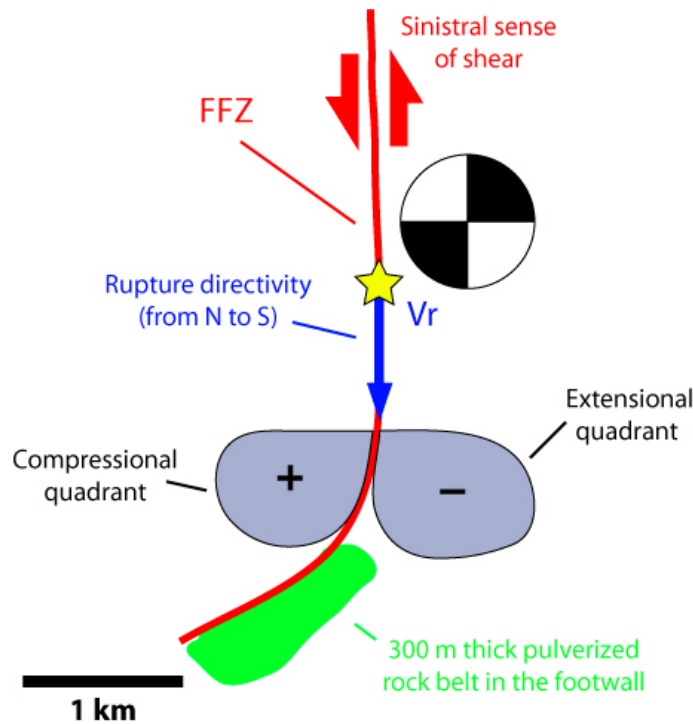

Fig. 6.1: A very conceptual scheme of the speculative interpretation of the damage zone in the outcrop 1 (Carnalez).

6.3.2 Rupture simulations along strike-slip faults and FFZ architecture

Ma and Andrews (2010) performed three-dimensional finite element simulations of dynamic ruptures along a strike-slip fault within an homogeneous elastic medium
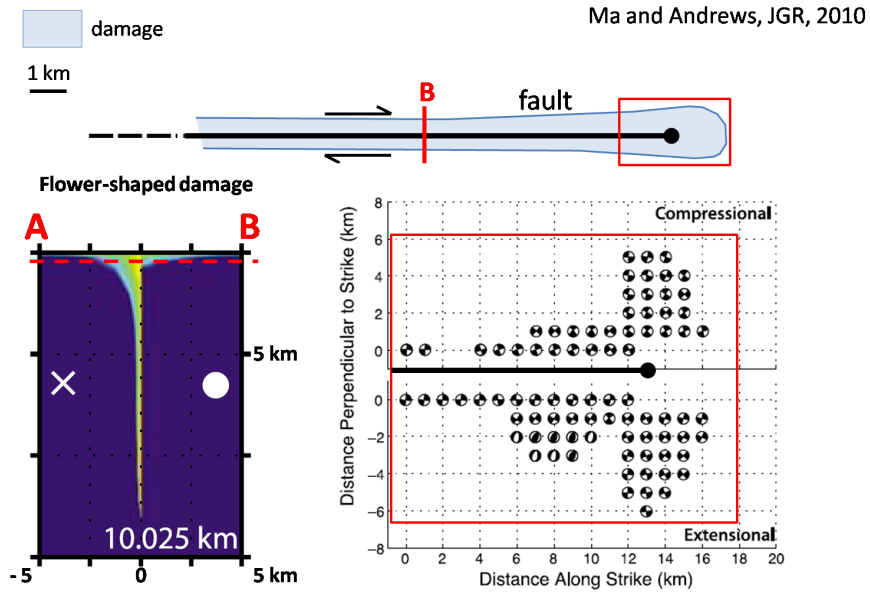
Fig. 6.2: The scheme shows the "flower-like" off-fault damage distribution (on the left) and the scattering of attitudes and kinematics of the secondary faults (on the right).

[Ma and Andrews, 2010]. Such medium was allowed to be inelastically deformed following a Drucker-Prageryield criterion (i.e., shear fracturing in 3D) due to stress perturbations associated to the passage of both the rupture tip and seismic wave fronts. This model predicts (i) an off-fault damage distribution with a "flower-like" shape (i.e., a broad damage zone near the surface that rapidly narrows with increasing confining pressure), and (ii) the formation of secondary faults/fractures with scattered attitudes and kinematics (reverse to normal) near the surface and sub-parallel faults/fractures with dominant strike-slip kinematics at depth (see Fig.6.2). The cumulative vertical throw across the FFZ was ca. 0.3 km at outcrop 1, near the southern fault tip, and progressively increased toward the north up to 1.5 km at outcrop 3. A possible assumption is that the exposed section of FFZ at outcrop 3 represented a deeper portion of the fault zone with respect to that exposed at outcrop 1. As a consequence, the structure of the FFZ would be qualitatively comparable with the theoretical results of Ma and Andrews (2010). Indeed moving from the southern, shallower portion to the northern, deeper portion of the FFZ, (i) the thickness of the fault zone reduced, (ii) the scattering of the attitude of the mirror-like faults decreased and (iii) the kinematics of the minor faults switched from dom-

inant dip-slip to dominant oblique- to strike-slip (consistently with the kinematics of the main fault). Summarizing, according to this interpretation,the distribution (thickness, attitude, etc.) of both "pulverized" dolostones and mirror-like faults along the FFZ resulted from off-fault coseismic damage due to the propagation of multiple earthquake ruptures.

6.3.3 Comparison of the architecture of the FFZ with active seismogenic sources in carbonate rocks

In the last few years increasingly high-resolution seismological techniques (e.g., high-precision hypocenters relocation, seismic tomography) yielded new constraints on the broad geometry of active seismogenic fault zones [Bressan et al., 2009, Chiaraluce et al., 2011, Valoroso et al., 2013].

For example, Bressan et al. (2009) analyzed the aftershocks of the 12 April 1998 $M_D = 5.6$ and the 12 July 2004 $M_D = 5.1$ Bovec-Krn earthquakes which nucleated along the NW-SE-trending dextral strike-slip Bovec-Krn fault (northwestern Slovenia) [Bressan et al., 2009]. By combining tomographic analyses of the fault zone with high-quality earthquake relocations they showed that the two main shocks and a majority of the aftershocks nucleated within platform limestones and dolomitic limestones between 2 and 10 km depth. They also showed that aftershocks were more or less symmetrically distributed with respect to the trace of the Bovec-Krn fault within a maximum distance of ca. 2 km from the fault trace. Variations in seismic wave velocities suggested that the fault zone contained branching and minor splay faults. In particular, the aftershock distribution of the 1998 earthquake was consistent with the activation of several sub-vertical surfaces broadly parallel to the NW-SE strike of the main fault. Instead, the 2004 aftershock sequence was characterized by a more diffuse pattern consistent with the activation of many minor fault surface sin a wide range of orientations. In both cases, many of the aftershock focal mechanisms showed fault plane solutions (strike-slip but also many normal and reverse events) and fault plane orientations different to those of the two main shocks (see Fig.6.3). Another significant study is that of Valoroso et al. (2013) which investigated in detail the anatomy of the normal fault system cutting carbonate host rocks where the 2009 L'Aquila earthquake ($M_w = 6.1$) propagated. This study was

based on the high-precision relocation of ca. 64000 earthquakes (both foreshocks and aftershocks) spanning over one year. Such a dataset allowed to reach a magnitude of completeness of 0.7 (more than 1 unit lower than other state-of-the-art earthquake catalogues) which let to image the fault architecture with a resolution of tens of meter and to resemble the complexity observed in exhumed fault zones by field geologists. One of the main results of this study was the definition of a seismological damage zone (SDZ), defined for each fault strand as the width enclosing 95% of the aftershocks distributions. The SDZ showed strong width variations along fault strike ranging from ca. 0.3 km in the portion of the fault where the mainshock nucleated to 1.5 km toward the southern fault tip where the rupture directivity was reported. Moreover, toward the fault tip, an increasing fault zone complexity was also reported which was characterized by the presence of (i) multiple antithetic and synthetic fault segments tens of meters long in both the hangingwall and the footwall, (ii) fault bends and jogs at different scales, and (iii) fault intersections along main faults and fault splays. All these observations compare well with many structural features reported within the exhumed seismogenic FFZ which was characterized by thicknesses comparable to those reported by Valoroso et al. and increasing complexity toward the fault tip. On the other hand, the presence of a stack of sub-parallel fault strands in the northern portion of the FFZ (at the Doss de la Ceora) is more consistent with the observations relative to the aftershock distribution around the Bovec-Krn strike-slip fault [Bressan et al., 2009]. Both the studies of Bressan et al. (2009) and Valoroso et al. (2013) highlighted the geometrical complexity of seismic fault zones going to the scale of the hundreds of meters. Based on the field observations conducted within the FFZ I can argue that a strong effect on geometrical complexity can be due to the coseismic reactivation of preexisting structures within highly anisotropic host rocks such as sedimentary carbonates. For example, in the case of the FFZ, many mirror-like slip surfaces (markers of seismic faulting) exploited the bedding surfaces of the dolostones (Fig.4.7).

The FFZ consisted of large volumes of "pulverized" dolostones (i.e., probably the result of coseismic damage) cut by mirror-like faults (i.e., markers of seismic slip, Fondriest et al., in press) but with scarse lateral continuity (20 m at maximum), also because of exposure limitations of some kind (extension of the outcrop, presence of
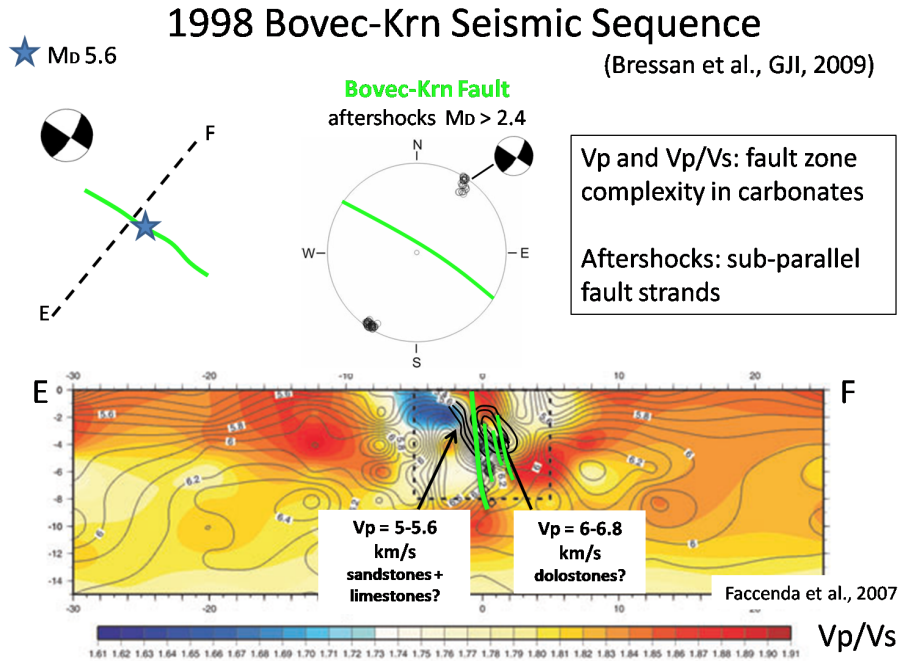
Fig. 6.3: Bovec-Krn seismic sequence of 1998, in which there was the activation of several sub-vertical surfaces broadly parallel to the NW-SE strike of the main fault, drawn in green on the image.

debris, etc.). The FFZ is exposed for 30 km along strike and may have hosted earthquake ruptures up to M_w 6.5 [Wells and Coppersmith, 1994]. On the other hand, if we estimate lengths of 30-300 m for individual fault mirror-like surfaces, they may have hosted earthquake ruptures up to M_w 2, associated to average coseismic slips of few centimeters at most. Therefore the exposed FFZ that I described in this thesis might record the cumulative history of all the past main seismic ruptures with their associated foreshock and aftershock sequences. This observation highlights the significant role of aftershock sequences in fault zone growth processes [Valoroso et al., 2013].

Chapter 7

Conclusions

Carbonate-cutting faults are significant seismic sources in all the Mediterranean area, including Italy. In this thesis I investigated from the km to the mm scale the architecture of a fault zone cutting carbonate rocks by using remote sensing structural analysis, detailed structural geology field survey and microstructural investigations. The case study was the Foiana Fault Zone (FFZ: Linea della Foiana *auctores*), a ca. 30 km long NNE-SSW striking sinistral transpressive fault zone in the Val di Non area (Italian Southern Alps). The FFZ cut through sedimentary dolostone of Triassic age and was estimated to be exhumed from a maximum depth of 2.5 km. At the kilometer scale the FFZ was characterized by a NE-SW trending restraining bend at the southern fault tip and by an increasing cumulative vertical throw in the range 0.3 - 1.5 km moving from the south to the north along fault strike (section 2). The aim of the study was the detailed description of the fault zone architecture and of the associated fault rocks with particular emphasis to the individuation of potential seismic markers (sections 3, 4 and 5). Here below I summarize the main results of my study:

- The FFZ consisted of intensely damaged dolostones that I distinguished between fragmented and highly fragmented dolostones. Field and microstructural observations suggested that such dolostones were shattered *in situ* without accommodating significant shear strain (sections 4 and 5). The *in situ* shattered dolostones showed characteristics (fragmented radial clasts, etc.) similar to pulverized rocks which were widely interpreted as the result of off-fault co-seismic damage in the wall rocks due to in-fault rupture propagation during

earthquakes [Dor et al., 2009]. We defined the shattered rocks as "pulverized" dolostones (section 6.1.1).

- The "pulverized" dolostones were cut by discrete faults characterized by mirror-like slip surfaces and associated ultracataclastic slip zones (sections 4 and 5). Mirror-like slip surfaces in dolostone gouges were demonstrated to be markers of seismic faulting since they were produced in rotary shear experiments only at seismic deformation conditions (section 6.1.2).

The above two main conclusions suggest that the FFZ was seismic in the Miocene (i.e., the FFZ cuts the Triassic Sciliar Fm. and its kinematics is consistent with the Valsugana deformation phase, 10 - 8 Ma , sections 2 and 3). As a consequence the FFZ architecture is an example of a seismogenic fault zone, with dolostone rocks in the footwall, exhumed from 1.5 - 2.5 km depth. We observed the following architectural features:

- The FFZ was characterized by significant changes in fault zone architecture. Moving along fault strike from the south (locality of Carnalez, fault exhumation depth of ca. 1.5 km), near the fault tip, to the north (locality of Doss de la Ceora, exhumation depth of ca. 2.5 km) (sections 3 and 4):

  - the thickness of the fault zone reduced from 300 m to less than 200 m;

  - the attitude of the minor faults (often with mirror-like surfaces) changed from scattered to dominant sub-vertical and sub-vertical;

  - the kinematics of the minor faults switched from dominant dip-slip reverse to dominant oblique- to strike-slip;

  - the "pulverized" dolostones were found in the footwall of the FFZ.

Given the ancient seismicity of the FFZ, we interpreted and discussed the above structural features as follows:

- The evolution of the architecture of the FFZ was strongly influenced by preexisting structures within the wall rocks, such as the bedding surfaces, which were frequently exploited by the faults. Given the presence of mirror-like surfaces,

the reactivation of preexisting anisotropies (in this case, bedding) is coseismic (section 6.2): earthquake dynamics controls the evolution, thickening and growth of the fault zone (section 6.3.3).

- The "pulverized" rocks were located in the footwall of the FFZ, which corresponds to the south-east tensional quadrant for a rupture propagating from north to south in a sinistral fault. This suggest preferential directivity (from north to the south) of the Miocene in age seismic ruptures. According to this interpretation, the southern restraining band acted as a barrier for the seismic ruptures (section 6.3.1).

- The peculiar architectural and kinematic features (switching from scattered fault attitudes in the southern part to sub-parallel in the northern part of the fault) are consistent with propagation of individual seismic ruptures according to earthquake numerical simulations [Ma and Andrews, 2010] (section 6.3.2).

- The architecture of the FFZ is an example of a seismogenic source in dolostone rocks and can be compared with high-resolution seismological and geophysical imaging of active seismogenic sources hosted in carbonate rocks [Bressan et al., 2009, Valoroso et al., 2013] (section 6.3.3).

Acknowledgements

Volevo prima di ogni cosa ringraziare Michele per tutto il tempo che gli ho fatto perdere, le mail tipo stalker e non ultima la sua ospitalità durante il lavoro di campagna. Grazie alla sua pazienza ed alle sue revisioni la tesi ha potuto avere un senso logico, e un inglese sicuramente comprensibile.

Ringrazio allo stesso modo anche il Prof. Di Toro, che nonostante i tentativi di farmi cambiare idea, continua a ricevere da me il "lei", abitudine che, mi sento di promettergli in questa sede, abbandonerò. Grazie di tutto Giulio, soprattutto delle telefonate degli ultimi giorni in cui il panico era ormai incontrollabile.

Ovviamente ringrazio i cari vecchi, Davide e Nadia miei finanziatori e affettuosi (soprattutto Nadia) e ironico-sarcastici (soprattutto Davide) motivatori. Ringrazio anche quelli ancora più vecchi: i nonni Amelia, Virgilio e Mirella. Ringrazio anche il "fratellino" Matteo. Ricordate che vi voglio bene, ve lo scrivo per bene anche perchè so che di questa tesi leggerete solo i ringraziamenti (forse).

Ringrazio tutti i miei amici, che non voglio elencare perchè rischierei di fare la pessima figura di dimenticare qualcuno, preso dalla situazione drammatica di fine scrittura della tesi. Ma sappiate che siete tutti nel mio cuore, da quando abbattei quell'albero qualche anno fa, ai giardini del paese, ed iniziai a mettere il naso fuori, nel mondo. Tutti gli amici del liceo, di cui solo pochi ho l'immensa fortuna di vedere ancora e non smettono mai di regalarmi grandi serate, e che, a distanza di 5 anni, mi dimostrano che sfatare il mito del fuori-liceo-non-sappiamo-che-dirci, è ancora possibile. Gli amici che ho incontrato a Padova e con cui ho fatto indimenticabili serate più o meno sobrie e geocene fantastiche, che ringrazio per l'ospitalità nella "big city". Gli amici che nei vari percorsi della mia vita recente sono arrivati, alcuni andati e più visti, a cui comunque voglio sempre bene e per loro rimarrà sempre spazio in me. Gli amici che sono andati, questi si per sempre, veramente troppo

giovani, e per cui conservo ricordo e sempiterna commozione, e meritano di essere
citati: Mea e Beppe. Carissimi amici sappiate che vi voglio immensamente bene e
che vi devo quasi tutto.

Quasi tutto perchè gran parte dello Stefano di adesso è dovuto alla mia Laura.
Cara Laura, ci laureeremo insieme, e voglio qui dirti semplicemente una cosa (che
in realtà sono due): ti amo.

Ringrazio infine tutti quelli che ho dimenticato di citare precedentemente, maledetta
la mia memoria.

Bibliography

[Abercrombie and Mori, 1996] Abercrombie, R. E. and Mori, J. (1996). Occurrence patterns of foreshocks to large earthquakes in the western United States.

[Agosta and Aydin, 2006] Agosta, F. and Aydin, A. (2006). Architecture and deformation mechanism of a basin-bounding normal fault in Mesozoic platform carbonates, central Italy. *Journal of Structural Geology*, 28(8):1445–1467.

[Avanzini et al., 2007] Avanzini, M., Bargossi, G., Borsato, A., Castiglioni, G., and Cucato, M. (2007). Note Illustrative della Carta Geologica d'Italia alla scala 1: 50.000, Foglio 026 Appiano. *Provincia Autonoma di Trento, Servizio Geologico. APAT-Servizio Geologico d'Italia, Roma.*

[Bargossi et al., 2004] Bargossi, G., Klötzli, U., Mair, V., Marocchi, M., and Morelli, C. (2004). The Lower Permian Athesian volcanic group (avg) in the Adige Valley between Merano and Bolzano: a stratigraphic, petrographic and geochronological outline. In *32nd International geological congress, Florence*, volume 187.

[Ben-Zion and Shi, 2005] Ben-Zion, Y. and Shi, Z. (2005). Dynamic rupture on a material interface with spontaneous generation of plastic strain in the bulk. *Earth and Planetary Science Letters*, 236(1):486–496.

[Billi et al., 2003] Billi, A., Salvini, F., and Storti, F. (2003). The damage zone-fault core transition in carbonate rocks: implications for fault growth, structure and permeability. *Journal of Structural Geology*, 25(11):1779–1794.

[Bouchon et al., 2010] Bouchon, M., Karabulut, H., Bouin, M.-P., Schmittbuhl, J., Vallée, M., Archuleta, R., Das, S., Renard, F., and Marsan, D. (2010). Faulting characteristics of supershear earthquakes. *Tectonophysics*, 493(3):244–253.

[Bressan et al., 2009] Bressan, G., Gentile, G., Perniola, B., and Urban, S. (2009). The 1998 and 2004 Bovec-Krn (Slovenia) seismic sequences: aftershock pattern, focal mechanisms and static stress changes. *Geophysical Journal International*, 179(1):231–253.

[Brune, 2001] Brune, J. (2001). Fault normal dynamic loading and unloading: an explanation for "non-gouge" rock powder and lack of fault-parallel shear bands along the San Andreas fault. *EOS Trans. Am. Geophys. Union*, 82:47.

[Cadrobbi, 1965] Cadrobbi, M. (1965). *Escursioni geologiche lungo la linea di Foiana (Valle di Non occidentale)*. Società Cooperativa Tipografica.

[Caine et al., 1996] Caine, J. S., Evans, J. P., and Forster, C. B. (1996). Fault zone architecture and permeability structure. *Geology*, 24(11):1025–1028.

[Castellarin and Cantelli, 2000] Castellarin, A. and Cantelli, L. (2000). Neo-Alpine evolution of the southern Eastern Alps. *Journal of Geodynamics*, 30(1):251–274.

[Castellarin et al., 2006] Castellarin, A., Vai, G. B., and Cantelli, L. (2006). The Alpine evolution of the Southern Alps around the Giudicarie faults: A Late Cretaceous to Early Eocene transfer zone. *Tectonophysics*, 414(1):203–223.

[Chester and Chester, 1998] Chester, F. M. and Chester, J. S. (1998). Ultracataclasite structure and friction processes of the Punchbowl fault, San Andreas system, California. *Tectonophysics*, 295(1):199–221.

[Chiaraluce et al., 2011] Chiaraluce, L., Valoroso, L., Piccinini, D., Di Stefano, R., and De Gori, P. (2011). The anatomy of the 2009 L'Aquila normal fault system (central Italy) imaged by high resolution foreshock and aftershock locations. *Journal of Geophysical Research: Solid Earth (1978–2012)*, 116(B12).

[Cowan, 1999] Cowan, D. S. (1999). Do faults preserve a record of seismic slip? A field geologist's opinion. *Journal of Structural Geology*, 21(8):995–1001.

[Dal Piaz, 1942] Dal Piaz, G. (1942). *Geologia della bassa valle d'Ultimo e del massiccio granitico di Monte Croce*. Tipografia Editrice Multilati e Invalidi.

[De Paola et al., 2011] De Paola, N., Hirose, T., Mitchell, T., Di Toro, G., Viti, C., and Shimamoto, T. (2011). Fault lubrication and earthquake propagation in thermally unstable rocks. *Geology*, 39(1):35–38.

[Di Toro et al., 2011] Di Toro, G., Han, R., Hirose, T., De Paola, N., Nielsen, S., Mizoguchi, K., Ferri, F., Cocco, M., and Shimamoto, T. (2011). Fault lubrication during earthquakes. *Nature*, 471(7339):494–498.

[Di Toro et al., 2005] Di Toro, G., Nielsen, S., and Pennacchioni, G. (2005). Earthquake rupture dynamics frozen in exhumed ancient faults. *Nature*, 436(7053):1009–1012.

[Di Toro et al., 2012] Di Toro, G., Smith, S., Fondriest, M., Bistacchi, A., Nielsen, S., Mitchell, T., Mittempergher, S., and Griffith, W. (2012). Is the fault core-damage zone model representative of seismogenic faults? Pre-existing anisotropies and fault zone complexity. In *2012 AGU Fall Meeting*, pages T24A–01. AGU.

[Doan and Billi, 2011] Doan, M.-L. and Billi, A. (2011). High strain rate damage of Carrara marble. *Geophysical Research Letters*, 38(19).

[Doan and Gary, 2009] Doan, M.-L. and Gary, G. (2009). Rock pulverization at high strain rate near the San Andreas fault. *Nature geoscience*, 2(10):709–712.

[Doglioni and Bosellini, 1987] Doglioni, C. and Bosellini, A. (1987). Eoalpine and mesoalpine tectonics in the Southern Alps. *Geologische Rundschau*, 76(3):735–754.

[Dor et al., 2006] Dor, O., Ben-Zion, Y., Rockwell, T. K., and Brune, J. (2006). Pulverized rocks in the Mojave section of the San Andreas Fault Zone. *Earth and Planetary Science Letters*, 245(3):642–654.

[Dor et al., 2009] Dor, O., Chester, J. S., Ben-Zion, Y., Brune, J. N., and Rockwell, T. K. (2009). Characterization of damage in sandstones along the Mojave section of the San Andreas Fault: Implications for the shallow extent of damage generation. *Pure and Applied Geophysics*, 166(10-11):1747–1773.

[Dor et al., 2008] Dor, O., Yildirim, C., Rockwell, T. K., Ben-Zion, Y., Emre, O., Sisk, M., and Duman, T. Y. (2008). Geological and geomorphologic asymmetry across the rupture zones of the 1943 and 1944 earthquakes on the North Anatolian Fault: possible signals for preferred earthquake propagation direction. *Geophysical Journal International*, 173(2):483–504.

[Faulkner et al., 2010] Faulkner, D., Jackson, C., Lunn, R., Schlische, R., Shipton, Z., Wibberley, C., and Withjack, M. (2010). A review of recent developments concerning the structure, mechanics and fluid flow properties of fault zones. *Journal of Structural Geology*, 32(11):1557–1575.

[Fondriest et al., 2013] Fondriest, M., Smith, S. A., Candela, T., Nielsen, S. B., Mair, K., and Di Toro, G. (2013). Mirror-like faults and power dissipation during earthquakes. *Geology*, pages G34641–1.

[Fondriest et al., 2012] Fondriest, M., Smith, S. A., Di Toro, G., Zampieri, D., and Mittempergher, S. (2012). Fault zone structure and seismic slip localization in dolostones, an example from the Southern Alps, Italy. *Journal of Structural Geology*.

[Graham et al., 2003] Graham, B., Antonellini, M., and Aydin, A. (2003). Formation and growth of normal faults in carbonates within a compressive environment. *Geology*, 31(1):11–14.

[Grohmann and Campanha, 2010] Grohmann, C. and Campanha, G. (2010). Openstereo: open source, cross-platform software for structural geology analysis. In *AGU Fall Meeting abstracts*, volume 1, page 06.

[Han et al., 2007] Han, R., Shimamoto, T., Hirose, T., Ree, J.-H., and Ando, J.-i. (2007). Ultralow friction of carbonate faults caused by thermal decomposition. *Scienc*, 316(5826):878–881.

[Hausegger et al., 2010] Hausegger, S., Kurz, W., Rabitsch, R., Kiechl, E., and Brosch, F.-J. (2010). Analysis of the internal structure of a carbonate damage zone: Implications for the mechanisms of fault breccia formation and fluid flow. *Journal of Structural Geology*, 32(9):1349–1362.

[King and Nábělek, 1985] King, G. and Nábělek, J. (1985). Role of fault bends in the initiation and termination of earthquake rupture. *Science*, 228(4702):984–987.

[Ma and Andrews, 2010] Ma, S. and Andrews, D. (2010). Inelastic off-fault response and three-dimensional dynamics of earthquake rupture on a strike-slip fault. *Journal of Geophysical Research: Solid Earth (1978–2012)*, 115(B4).

[Mitchell et al., 2011] Mitchell, T., Ben-Zion, Y., and Shimamoto, T. (2011). Pulverized fault rocks and damage asymmetry along the Arima-Takatsuki Tectonic Line, Japan. *Earth and Planetary Science Letters*, 308(3):284–297.

[Mitchell and Faulkner, 2009] Mitchell, T. and Faulkner, D. (2009). The nature and origin of off-fault damage surrounding strike-slip fault zones with a wide range of displacements: a field study from the Atacama fault system, northern Chile. *Journal of Structural Geology*, 31(8):802–816.

[Niemeijer et al., 2012] Niemeijer, A., Di Toro, G., Griffith, W. A., Bistacchi, A., Smith, S. A., and Nielsen, S. (2012). Inferring earthquake physics and chemistry using an integrated field and laboratory approach. *Journal of structural geology*, 39:2–36.

[Prosser, 2000] Prosser, G. (2000). The development of the North Giudicarie fault zone (Insubric line, Northern Italy). *Journal of Geodynamics*, (30):229–250.

[Reches and Dewers, 2005] Reches, Z. and Dewers, T. A. (2005). Gouge formation by dynamic pulverization during earthquake rupture. *Earth and Planetary Science Letters*, 235(1):361–374.

[Rempe et al., 2013] Rempe, M., Mitchell, T., Renner, J., Nippress, S., Ben-Zion, Y., and Rockwell, T. (2013). Damage and seismic velocity structure of pulverized rocks near the San Andreas Fault. *Journal of Geophysical Research: Solid Earth*.

[Riedel, 1929] Riedel, W. (1929). Zur mechanik geologischer brucherscheinungen. *Zentralblatt für Mineralogie, Geologie und Paläontologie B*, 1929:354–368.

[Rockwell et al., 2010] Rockwell, T., Sisk, M., Girty, G., Dor, O., Wechsler, N., and Ben-Zion, Y. (2010). Chemical and physical characteristics of pulverized Tejon Lookout Granite adjacent to the San Andreas and Garlock faults: implications for earthquake physics. In *Mechanics, Structure and Evolution of Fault Zones*, pages 1725–1746. Springer.

[Schmid et al., 1989] Schmid, S., Aebli, H., Heller, F., and Zingg, A. (1989). The role of the Periadriatic Line in the tectonic evolution of the Alps. *Geological Society, London, Special Publications*, 45(1):153–171.

[Scholz, 2002] Scholz, C. H. (2002). *The mechanics of earthquakes and faulting*. Cambridge university press.

[Sibson, 1977] Sibson, R. (1977). Fault rocks and fault mechanisms. *Journal of the Geological Society*, 133(3):191–213.

[Sibson, 2003] Sibson, R. H. (2003). Thickness of the seismic slip zone. *Bulletin of the Seismological Society of America*, 93(3):1169–1178.

[Siman-Tov et al., 2013] Siman-Tov, S., Aharonov, E., Sagy, A., and Emmanuel, S. (2013). Nanograins form carbonate fault mirrors. *Geology*, 41(6):703–706.

[Smith et al., 2013] Smith, S., Di Toro, G., Kim, S., Ree, J.-H., Nielsen, S., Billi, A., and Spiess, R. (2013). Coseismic recrystallization during shallow earthquake slip. *Geology*, 41(1):63–66.

[Smith et al., 2011] Smith, S. A., Billi, A., Di Toro, G., and Spiess, R. (2011). Principal slip zones in limestone: microstructural characterization and implications for the seismic cycle (Tre Monti Fault, Central Apennines, Italy). *Pure and Applied Geophysics*, 168(12):2365–2393.

[Valoroso et al., 2013] Valoroso, L., Chiaraluce, L., Piccinini, D., Di Stefano, R., Schaff, D., and Waldhauser, F. (2013). Radiography of a normal fault system by 64,000 high-precision earthquake locations: The 2009 L'Aquila (central Italy) case study. *Journal of Geophysical Research: Solid Earth*, pages 1–21.

[Viganò et al., 2011] Viganò, A., Tumiati, S., Recchia, S., Martin, S., Marelli, M., and Rigon, R. (2011). Carbonate pseudotachylytes: evidence for seismic faulting along carbonate faults. *Terra Nova*, 23(3):187–194.

[Viola et al., 2001] Viola, G., Mancktelow, N. S., and Seward, D. (2001). Late Oligocene-Neogene evolution of Europe-Adria collision: New structural and geochronological evidence from the Giudicarie fault system (Italian Eastern Alps). *Tectonics*, 20(6):999–1020.

[Wells and Coppersmith, 1994] Wells, D. L. and Coppersmith, K. J. (1994). New empirical relationships among magnitude, rupture length, rupture width, rupture area, and surface displacement. *Bulletin of the Seismological Society of America*, 84(4):974–1002.

[Wesnousky, 2006] Wesnousky, S. G. (2006). Predicting the endpoints of earthquake ruptures. *Nature*, 444(7117):358–360.

[Wibberley et al., 2008] Wibberley, C. A., Yielding, G., and Di Toro, G. (2008). Recent advances in the understanding of fault zone internal structure: A review. *Geological Society, London, Special Publications*, 299(1):5–33.

[Wilson et al., 2005] Wilson, B., Dewers, T., Reches, Z., and Brune, J. (2005). Particle size and energetics of gouge from earthquake rupture zones. *Nature*, 434(7034):749–752.

[Yuan et al., 2011] Yuan, F., Prakash, V., and Tullis, T. (2011). Origin of pulverized rocks during earthquake fault rupture. *Journal of Geophysical Research: Solid Earth (1978–2012)*, 116(B6).